Antenna Array and Waveform Design for 4D-Imaging mmWave MIMO Radar Sensors

Nazila Karimian-Sichani*[1], Mohammad Alaee-Kerahroodi[2],
Bhavani Shankar M. R.[2], Esfandiar Mehrshahi[1], Seyed Ali Ghorashi[3]

[1]*Department of Telecommunications, Faculty of Electrical Engineering, Shahid Beheshti University, Tehran 1983963113, Iran.*
[2]*Interdisciplinary Centre for Security, Reliability and Trust (SnT), University of Luxembourg, Luxembourg.*
[3]*Department of Computer Science and Digital Technologies, School of Architecture, Computing and Engineering, University of East London, E16 2RD, London, UK.*

***Abstract*—The emerging 4D-Imaging mmWave MIMO radars have significant advantages over conventional radar sensors. However, the physical placement of transmit and receive antennas to achieve the desired virtual array, while considering cost and efficiency is not intuitive. Furthermore, due to the large number of transmit elements used in such systems, they necessitate the appropriate strategy for transmit waveforms selection and design, which should be separable on the receive side in addition to having low auto-correlation sidelobes. In this paper, we propose a general optimization framework based on Coordinate Descent (CD), to solve the problems of antenna array and waveform design for 4D-imaging radar sensors. First, we propose the CD approach for an optimal array configuration design. The proposed framework obtains a sequence of optimal antenna placements. The objective function converges to a solution that guarantees the desired number of transmit and receive antenna elements, while the obtained virtual array is as close to the desired virtual array as possible. We, then, propose an entry-based optimization framework based on our optimization framework, CD, to jointly design a phase-modulated constant modulus waveform set that is optimized based on weighted integrated sidelobe level and spectrum shaping, considering the radar is working adjacent to communication systems. Finally, the simulation results are provided to assess the validity of our proposed methods for both array and waveform design. The former is validated by simulating the virtual array of several commercially available 4D-Imaging radar products. The latter demonstrates that our proposed waveform design can outperform conventional MIMO-FMCW approaches, by performing comparative simulations. Finally we show that it can also provide compatibility with other communication systems.**

***Index Terms*—4D-Imaging, Automotive Radar, PMCW, CDM-MIMO, WISL, waveform design, spectrum shaping.**

I. Introduction

The emerging 4D-Imaging millimeter-Wave (mmWave) radar sensors, as a high-resolution technology, offer significant advantages over 3D radars and are being widely employed in different applications including in-cabin sensing, indoor sensing, health care, and autonomous driving. Considering an example of automotive application, 4D-Imaging mmWave radars are the next-generation radar systems that demonstrate new ways for Highly Automated Driving (HAD) to improve automotive safety [1]–[5]. Due to the requirement of high-resolution sensing capability in the range–Doppler–azimuth–elevation domains, HAD systems require high resolution 4D-Imaging radars to provide high angular resolution and better Direction Of Arrival (DOA) estimation. For a high angular resolution in both azimuth and elevation a large antenna array aperture size and also a large number of transmit and/or receive channels are required.

The state-of-the-art automotive radars use Multiple-Input Multiple-Output (MIMO) radar concept [6] as an attractive alternative to the full sensor array. For 4D-Imaging radars, a large number of antenna elements, such as a planar array with 576 elements, are required, resulting in a significant cost for a radar sensor if the antenna elements are built physically [7]. Alternatively, the physical elements can be efficiently created virtually, if sparse array configuration be used on one side of the transmit (Tx) or receive (Rx) chain.[1]. The virtual array in MIMO setting is obtained by convolving the locations of transmitter and receiver elements. Hence, the properties of the virtual array are affected by the physical placement of transmitting and receiving elements [14]. In this context, some considerations should be taken into account, such as the distance and the number of transmitter and receiver array elements. Mutual coupling effects distort MIMO emissions, when the antenna elements are electrically close (less than half-wavelength spacing). On the other hand, the inter-element spacing (d) greater than a half wavelength between antenna elements will lead to grating lobes [15]. To avoid the grating lobes, we need to design a filled virtual array with half wavelength spacing between array elements.

On the other hand, antenna allocation and configuration in colocated MIMO radar plays an important role in the resource-aware design of autonomous driving systems. In mmWave radar sensors, the receive chains are sometimes more expensive than the transmit chains [4]. Each receiving element requires an Analog to Digital Converter (ADC), which increases the hardware cost comparing with the transmit

*This paper was developed while Nazila Karimian-Sichani was visiting SPARC at SnT, University of Luxembourg. This work was supported by FNR CORE INTER project SENCOM: C20/IS/14799710/SENCOM, and FNR CORE R4DAR project C23/IS/18049793/R4DAR.

[1]It is essential to clarify that sparse arrays and sparsity in the context of compressed sensing are separate concepts. In this context, when we refer to sparse arrays, we mean an array of antennas with numerous zero elements [7]–[13]. On the other hand, sparsity in compressed sensing pertains to the property of signals being effectively approximated using only a small number of non-zero coefficients in a suitable basis.

element [9]. While being mass-produced, each sensor must be as inexpensive as possible. Thus, it would be required to select the minimum possible number of receive antenna elements and a reasonable number for transmit ones, as well as their placement to obtain a desired virtual array.

The 4D-imaging sensors not only require appropriately *antenna array design*, but also they require a good strategy of *waveform selection*. The large number of transmit antennas in 4D-Imaging radar sensors enlarges the complexity of the transmit waveforms, which is a subject of discussion in Frequency-Modulated Continuous-Wave (FMCW) and Phase-Modulated Continuous-Wave (PMCW) radar systems. The choice of waveform in the automotive MIMO radars is critical because it influences both radar performance and implementation complexity. In order to increase the radar performance, MIMO radar waveforms should possess good resolution, low sidelobes and orthogonality. Due to inevitable interference with other sensors in high resolution radars, they are also required to be capable of spectrum sharing [16].

In order to differentiate the signals emitted from different transmitters of the MIMO radar at the receiver, the transmitted signals should be orthogonal, which can be achieved in the time, frequency, or coding domains. To this end, different modulation schemes were presented in the literature, such as Time Division Multiplexing (TDM), Frequency Division Multiplexing (FDM), Doppler-Division Multiplexing (DDM), and Code-Division Multiplexing (CDM). Generating orthogonality is a difficult task to achieve in FMCW radars and leads to some drawbacks corresponding to each multiplexing technique. These drawbacks include increasing in the measurement time or bandwidth, loss of transmit power or waste of frequency resources, noticeable degradation in maximum unambiguous velocity, corruption in DOA estimation and reduction in the radar performance, to name a few [17]–[28].

On the other hand, orthogonal codes allow us to transmit orthogonal waveforms from all transmitters in PMCW MIMO radars simultaneously. This is achieved by the fast-time CDM-MIMO based on intra-pulse coding, which utilizes set of sequences with good auto- and cross-correlation properties [13], [29]–[36]. This scheme is a suitable solution for fast 4D-Imaging automotive applications, since it supports simultaneous transmitting in both time and frequency. The advantage of using CDM is that it overcomes the above-mentioned drawbacks for multiplexing in slow-time domain, and achieves higher SNR and higher range resolution in comparison with TDM and FDM, respectively. However, it suffers from difficult hardware implementation. Also, due to the cross-correlation among the codes, it is difficult to achieve perfect orthogonality, unlike TDM and FDM. Thus, the properties of the code set such as auto- and cross-correlation highly influence the performance of the CDM. The noise floor and range ambiguity limit the radar performance in the case of CDM. To adequately distinguish between the multiple targets, the codes should have very low cross-correlation values. The multiple-source interference levels are controlled by the cross-correlation as well as the relative power level of the received signals.

In addition to small cross-correlation levels requirement, transmit waveforms are required to provide compatibility with other sensors based on their spectrum utilization. By increasing the demand of installing multiple radars in every car at near future, the spectrum will be crowded. Hence, the problem of coexistence of radar and other sensors such as communication sensors, (RadCom) as another possibility in future, has received a major attention in recent cognitive MIMO radar systems. To tackle the spectrum congestion problem, the radar waveform should have the possibility of making itself adaptive to the environment [37]–[42]. Spectrum shaping and nulling the desired stop-bands in waveform design problem can enable the compatibility between radar and other sensors.

A. Background and Related Works

1) *Array Design*: Recently, some researches on the antenna array design and placement have been carried out. A new 2D planar antenna array design was introduced in [3] that enables the three dimensional object detection in 4D-Imaging application by creating a wide Field of View (FoV) in azimuth direction. In [11] imaging performance in a 3D-Imaging radar improved by using antenna array sparsity which is achieved by a two step synthesis procedure. The number of elements is reduced while improving angular resolution. Furthermore, by adjusting the antenna positions, the lowest possible sidelobe level is achieved. The Vayyar Walabot-60 GHz radar, which has a dense planar virtual MIMO array with a half-wavelength antenna spacing by default, is used to confirm the model. In [5] a system has been proposed with 36 Tx and 48 Rx channels, resulting in 1728 virtual channels, working in 79 GHz frequency. This antenna array is realized with 12×6 Monolithic Microwave Integrated Circuits (MMIC)s, providing a high resolution in both azimuth and range. In [14] a characterization of a nonuniform mmWave antenna array configuration for a MIMO radar sensor in a multistatic scenario was carried out. The authors employed a genetic algorithm to find the optimal antenna placement and used the ambiguity function as a metric to evaluate the DOA estimation performance of the fabricated prototype of the antenna system. In [43] in a similar work, considering the lack of the analytically solved inverse mapping from the virtual array to the real transmitter-receiver configuration, the authors proposed a genetic algorithm to search the optimal antenna placement based on the ambiguity function and the antenna beampattern.

In [44] the problem of joint array and waveform optimization was addressed to improve the angle estimation performance. To this end, Cramer-Rao-Based waveform correlation optimization in a MIMO radar given the geometries of transmitting and receiving antenna array, was investigated. In [45] by adding more Degree Of Freedom (DOF) to the problem of beampattern matching design using a binary antenna position vector, again the problem for joint optimization of the waveform covariance matrix and the antenna position vector was studied. The authors first optimize the covariance matrix by the Semidefinite Quadratic Programming (SQP) algorithm for a fixed antenna position vector, and then update the position vector using Alternating Direction Method of Multipliers (ADMM) for a fixed covariance matrix, iteratively.

A similar work has been carried out in [46] by a novel cyclic algorithm based on the non-convex formulation of the problem. In [10], the co-design problem of waveform covariance matrix and antenna positions with flexible response control was formulated to pursuit enhanced angle-estimation performance. Besides, a different optimization criterion, focusing on controlling mainlobe ripple and sidelobe level of the beampattern, was formulated to optimize the transmit beampattern. In [47] a new technique to find the optimal antenna array configuration in the problem of beampattern matching design was investigated by iteratively turning off the least important antennas in a Uniform Linear Array (ULA) setup and solving the corresponding SQP beam-pattern matching problem until a predefined number of antennas remain active.

The majority of studies in the literature, discussed above, have focused on the problem of beampattern matching design with a ULA setup, and antenna selection is accomplished by selecting N from M antennas and iteratively determining the best antenna position vector via optimization techniques. To the best of our knowledge, the problem of obtaining transmit and receive antenna positions for a desired virtual array elements configuration is not analytically solved yet, which is our discussion in the following sections.

2) *Waveform selection and Design*: As we discussed above, the choice of waveform in 4D-Imaging mmWave MIMO radars is critical because it influences both radar performance and implementation complexity. MIMO radar waveforms should possess low auto-correlation sidelobes, and be chosen from an orthogonal set to be separated in the receive side. Different modulation schemes, such as TDM [17]–[22], FDM [23], DDM [22], [24]–[26], [28], (slow-time) CDM (such as Binary Phase Modulation (BPM) and Hadamard coding) [22], [27] and their variations, have been presented in the literature to generate a set of orthogonal waveforms based on FMCW. Creating orthogonal signals in slow-time domain leads to a degradation in performance of the radar system as discussed above. The drawbacks of using these slow-time multiplexing techniques become more severe with the increase in the number of transmit antenna elements. Thus, in 4D-imaging automotive radars, due to the requirement of large number of transmit antenna elements, slow-time multiplexing becomes inefficient.

Another orthogonalization scheme that is used recently in automotive radars, is based on fast-time CDM, which in principle is suitable for PMCW radars [33]–[36]. CDM-MIMO based on intra-pulse coding, which is a systematic approach in many different radar applications, and utilizes set of sequences with good auto- and cross-correlation properties [29]–[32], [34]. This scheme is a suitable solution for fast 4D-Imaging mmWave applications, since it supports simultaneous transmitting in both time and frequency. The advantage of using CDM is that it overcomes the above-mentioned drawbacks for TDM, FDM, or BPM, and achieves higher SNR and higher range resolution in comparison with TDM and FDM, respectively. However, it suffers from difficult hardware implementation. Also, due to the cross-correlation among the codes, it is difficult to achieve perfect orthogonality, unlike TDM and FDM. Thus, the properties of the code set such as auto-correlation and cross-correlation highly influence the performance of the CDM. The noise floor and range ambiguity limit the radar performance in the case of CDM. To adequately distinguish between the multiple targets, the codes should have very low cross-correlation values. The multiple-source interference levels are controlled by the cross-correlation level as well as the relative power level of the received signals. Hence, finding a code set that satisfies the radar system requirement is challenging, but has been well studied and addressed in several recent papers.

There are several metrics available for designing a set of sequences with good orthogonality in PMCW radars [48], one of which is Integrated Side-lobe Level (ISL) and Weighted Integrated Side-lobe Level (WISL) [34]. For the MIMO radar, several approaches are proposed to design a set of sequences with small auto- and cross-correlation sidelobes based on the ISL minimization, including Multi-Cyclic Algorithm New (CAN)/Multi-PeCAN [49], Iterative Direct Search [50], ISLNew [51], Majorization-Minimization (MM)-Corr, [52] and Coordinate Descent (CD) [33], [53].

Due to the spectrum congestion in spectrally crowded environments, the problem of adaptive waveform design for coexistence of radar and telecommunication systems has been studied in recent cognitive MIMO radar systems. To enable compatibility between radar and communication systems, several waveform optimization methods have been investigated based on MM, CD, ADMM etc., [38]–[42], [54]–[59]. In [54], the problem of minimizing range-ISL with compatible spectral response under discrete phase constraint, has been considered and solved using CD to obtain the local optimum solution. In [55] the ISI and Peak to-average Power Ratio (PAPR) constraints are forced on the probing waveform and the problem is defined to reduce the mutual interference induced by the overlaid communication services. Then, the recast problem is formulated into a new ADMM form to tackle the resulting NP-hard problem. In [56] the authurs investigated the problem of the spectrally compatible waveform design for MIMO radar transmit beampattern formation, subject to PAPR and similarity constraints. Since the formulated optimization problem of minimizing the ISI and the waveform energy of the stop-band frequencies is NP–hard, the approximated-ADMM algorithm is proposed to tackle the resulting bi–quasiconvex problem. In [60] a waveform optimization model accounting for the minimization of the beampattern-ISI along with the mainlobe width, PAPR, and energy constraints, as well as multi-spectral requirements using a polynomial-time Sequential Convex Approximation (SCA) procedure is proposed to monotonically decrease the ISL. In [58] the problem of spectrally compatible waveform design for large-scale MIMO radar with one-bit Digital to Analog Converter (DAC)s is investigated. The auturs have formulated the beampattern matching design problem subject to spectral constraints and developed an AltOpt method using ADMM framework to optimize transmit waveforms with good spatial and frequency behavior.

B. Contribution

The contribution of this paper is divided into two parts, considering a full system of 4D-Imaging radar sensors design

point of view. First, as discussed above, we address the array design problem. In this context, we computationally address this gap, by proposing a framework for designing arbitrary virtual arrays.

The second part is dedicated to the problem of orthogonal set design and waveform optimization for automotive radar sensors in spectrally crowded environments. To this end, we propose an entry-based optimization approach to create an spectrally compatible orthogonal set of sequences for PMCW-MIMO radars suitable for automotive radars. The contributions of this work are summarized as follows:

- We formulate the problem of designing a MIMO virtual array that aims at minimizing the Mean-Squared-Error (MSE) between the designed virtual array and a given one, while antenna elements are assumed to be placed in a grid-point planar configuration. To design the virtual array with a specified number of Tx/Rx array elements, we consider minimizing the difference between the number of designed and desired array elements.
- We propose an iterative method based on the CD algorithm to solve the formulated optimization problem. With employing a scaling factor, the output of each iteration is used as an input for the next iteration.
- The simulation results show that the proposed method with a monotonically decreasing cost function, leads to the optimum binary Tx/Rx position matrices at its convergence.
- In the context of waveform design for 4D-imaging MIMO PMCW radars, we build upon our prior work as presented in [61]. Precisely, we introduce an unconstrained optimization problem in the Fourier domain. The objective is to design a set of spectrally compatible sequences that exhibit good orthogonality and low sidelobe levels in their correlation functions within a specified Regions Of Interest (ROI). This is achieved by optimizing the WISL metric. To enable spectrum shaping, we incorporate a weight vector into the problem. In contrast to our work in [61], where we addressed the problem under a continuous-phase constraint, we now propose a comprehensive algorithm that not only provides a solution for the continuous-phase constraint but also offers a direct solution for the discrete phase constraint. In essence, this approach encompasses both scenarios, ensuring a generic solution for sequence design in 4D-imaging MIMO PMCW radars.
- We use CD framework to solve the entry-based problem both for continuous-phase and discrete-phase constraints to design a constant modulus set of sequences. Through our proposed method we find the global solution to the sequence phases in each step of our CD approach that leads to a monotonically decreasing objective function until the convergence criterion is met.
- The numerical results validate the proposed algorithm's performance for a 4D imaging radar example.

C. Organization and Notation

The rest of this paper is organized as follows. In Section II the optimization framework which is used in this paper is discussed. In Section III the problem of MIMO virtual array design will be addressed and the problem formulation and the related optimization is discussed. Our proposed waveform design problem for PMCW-MIMO radars is provided in Section IV. To assess the validity and performance of our proposed techniques, Section V is dedicated to simulation results and numerical examples. Finally, Section VI provides conclusion to the paper.

Notation: $\mathbb{R}^N$ denotes the N-dimensional real vector space. We use boldface upper case $\mathbf{X}$ for matrices and boldface lower case $\mathbf{x}$ for vectors. $vec(.)$ is the vectorization operator. $||.||_F$ and $||.||_0$ are the Frobenius and zero norm of the matrix $\mathbf{X}$, respectively. Also, the (m,n)-th element of a matrix is denoted by $\mathbf{X}_{m,n}$. The transpose operator is denoted by $(.)^T$. $|x|$ denotes modulus of the complex number x and $|\mathbf{x}|$ is a vector of element wise absolute values of $\mathbf{x}$, i.e., $|\mathbf{x}| = \left[|x_1|, |x_2|, \ldots, |x_L|\right]^T$. The sets of complex number, real number, Hadamard product, Frobenius norm, phase of vector and matrix, hermitian operation, correlation, gradient, round and rectangular functions are denoted by, $\mathbb{C}^N$, $\mathbb{R}^N$, $\Im(.)$, $\odot$, $||.||_F$, $\angle.$, $(.)^H$, $\circledast$, ∇, $\lfloor . \rfloor$ and $rect(.)$ respectively. $\ln$ defines the natural logarithm.

II. Optimization Framework

In this section, to solve the problems defined later in this paper, we use an optimization framework based on CD which is briefly described here. The interested reader can refer to [12] for more details. The CD approach is a special case of Block Coordinate Descent (BCD), when we optimize a single variable in each step rather than a block of variables. Then, we solve the optimization problem alternatively with respect to each single variable while maintaining the others fixed. Usually, this results in sub-problems that are much easier to solve than the original problem. Consider the following single variable-structured non-convex optimization problem,

$$\mathcal{P}_{\mathbf{x}} \begin{cases} \min\limits_{x_n} & f(x_1, \ldots, x_N) \\ s.t. & x_n \in \mathcal{X}_n, \ \forall n = 1, \ldots, N \end{cases} \tag{1}$$

where $f(.) : \prod_{n=1}^{N} \mathcal{X}_n \to \mathbb{R}$, $\mathcal{X}_n, n = \{1, ..., N\}$ is a closed convex set, and each x_n is a single variable. The CD algorithm chooses an index n, at each iteration and updates x_n such that the objective function decreases. Thus, at the i^{th} iteration, N optimization problems are solved with the following form,

$$\mathcal{P}_{x_n}^{i+1} \begin{cases} \min\limits_{x_n} & f(x_n; \mathbf{x}_{-n}^{i}) \\ s.t. & x_n \in \mathcal{X}_n \end{cases} \tag{2}$$

where, $x_n, n \in \{1, \ldots, N\}$, is the current variable to be optimized and $\mathbf{x}_{-n}^{i}$ denotes the rest of the variable blocks at the i^{th} iteration. The selection of variables in each iteration is based on different rules, such as Cyclic, Randomized and Greedy for updating the variable blocks.

Due to the nature property of CD that ensures the objective function values monotonically decrease at each iteration such that $f\left(x^0\right) \geq f\left(x^1\right) \geq f\left(x^2\right) \geq \cdots$, the convergence of the objective function is guaranteed as long as it is bounded

Algorithm 1 CD Method.

1: **Inputs**: Initialization.
2: **Outputs**: Optimized decision vector $\mathbf{x}^{\star}$.
3: **for** $i = 0, 1, 2, \ldots$ **do**
4: Select indices order in the set N;
5: Optimize the n^{th} coordinate $\forall n \in N$, that is,
6: $x_n^{(i+1)} = \arg\min_{x_n \in \mathcal{X}_n} \{f(x_n; \mathbf{x}_{-n}^{(i)})\}$;
7: Stop if convergence criterion is met;
8: **end for**
9: **Outputs**: $\mathbf{x}^{\star} = \mathbf{x}^{(i+1)}$.

from below over the feasible set. If $f(.)$ is strictly convex and smooth, the CD algorithm converges to the global optimal solution. **Algorithm 1** summarizes the CD method.

III. MIMO Virtual Array Design Problem

A. Problem Formulation

We consider the problem of designing the configuration of Tx and Rx array antenna elements, in order to achieve a desired MIMO virtual array. Let $\mathbf{P}_t \in \{0,1\}^{M_t \times N_t}$ and $\mathbf{P}_r \in \{0,1\}^{M_r \times N_r}$ be defined as the Tx and Rx array antenna elements positions, respectively. Here, we assume a Uniform Rectangular Array (URA), i. e., a 2D planar configuration, for Tx and Rx antenna elements with M_t and N_t (M_r and N_r) as the dimensions of Tx (Rx) array elements position matrix, in the coordinate plane with equal grid spacing $d = \lambda/2$, where $t_{\tilde{i},\tilde{j}} \in \{0,1\}$ and $r_{\bar{i},\bar{j}} \in \{0,1\}$ denote the position of the $(\tilde{i},\tilde{j})^{th}$ Tx and $(\bar{i},\bar{j})^{th}$ Rx array element, respectively, and λ is the wavelength of the transmitted signal. $t_{\tilde{i},\tilde{j}} = 1$ (or $r_{\bar{i},\bar{j}} = 1$) indicates that a Tx (or Rx) antenna element is placed on the $(\tilde{i},\tilde{j})^{th}$ (or $(\bar{i},\bar{j})^{th}$) grid point location of the URA; otherwise $t_{\tilde{i},\tilde{j}} = 0$ (or $r_{\bar{i},\bar{j}} = 0$). The MIMO virtual array ($\mathbf{V}$) is constructed by convolving the locations of the real Tx and Rx as $\mathbf{V} = \mathbf{P}_t * \mathbf{P}_r$ [62]. Due to overlap between antennas in virtual array elements, thus $\mathbf{V} =\in \mathbb{Z}^{+^{(M_t+N_t-1)\times(M_r+N_r-1)}}$.

In order to design the MIMO virtual array with a required number of Tx/Rx array elements, we define the following optimization problem:

$$\begin{cases} \min\limits_{\mathbf{P_t},\mathbf{P_r},\alpha} & ||\mathbf{V}_d - \alpha \mathbf{P}_t * \mathbf{P}_r||_F \\ & \mathbf{P}_t(\tilde{i},\tilde{j}) = \{0,1\}, \\ & \forall \tilde{i} \in \{1,...,M_t\}, \tilde{j} \in \{1,...,N_t\} \\ & \big|||\mathbf{P}_t||_0 - L_T\big| < \zeta, \\ s.t. & \\ & \mathbf{P}_r(\bar{i},\bar{j}) = \{0,1\}, \\ & \forall \bar{i} \in \{1,...,M_r\}, \bar{j} \in \{1,...,N_r\} \\ & \big|||\mathbf{P}_r||_0 - L_R\big| < \zeta. \end{cases} \tag{3}$$

where $\mathbf{V}_d \in \mathbb{Z}^{+^{(M_t+N_t-1)\times(M_r+N_r-1)}}$ is the desired MIMO virtual array and α is a scaling parameter that should be optimized. The objective function is defined as a Frobenius norm of the distance between a desired virtual array and the designed one. L_T and L_R are the required number of Tx and Rx elements, respectively. The constraints $\big|||\mathbf{P}_t||_0 - L_T\big| < \zeta$ and $\big|||\mathbf{P}_r||_0 - L_R\big| < \zeta$ state that the distances between the number of designed and desired array elements, for both TX and RX, respectively, should be less than the threshold ζ.

This problem is a NP-hard non-convex optimization problem, due to the discrete (binary) and non-convex set of constraints ($\mathbf{P}_t(\tilde{i},\tilde{j}) = \{0,1\}, \forall \tilde{i} \in \{1,...,M_t\}, \tilde{j} \in \{1,...,N_t\}$ and $\mathbf{P}_r(\bar{i},\bar{j}) = \{0,1\}, \forall \bar{i} \in \{1,...,M_r\}, \bar{j} \in \{1,...,N_r\}$). To solve the problem, we re-arrange the problem into the penalty-based optimization framework, in order to design the MIMO virtual array and achieving the required number of Tx/Rx array elements simultaneously,

$$\begin{cases} \min\limits_{\mathbf{P_t},\mathbf{P_r},\alpha} & g_1 + \eta g_2 \\ & \mathbf{P}_t(\tilde{i},\tilde{j}) = \{0,1\}, \\ & \forall \tilde{i} \in \{1,...,M_t\}, \tilde{j} \in \{1,...,N_t\} \\ s.t. & \\ & \mathbf{P}_r(\bar{i},\bar{j}) = \{0,1\}, \\ & \forall \bar{i} \in \{1,...,M_r\}, \bar{j} \in \{1,...,N_r\} \end{cases} \tag{4}$$

where,

$$g_1 = ||\mathbf{V}_d - \alpha \mathbf{P}_t * \mathbf{P}_r||_F, \tag{5}$$

$$g_2 = \big(\big|||\mathbf{P}_t||_0 - L_T\big| + \big|||\mathbf{P}_r||_0 - L_R\big|\big). \tag{6}$$

$\eta \in [0,1]$ is a scaling factor and with this form, we can achieve a desired virtual array with the specified number of Tx and Rx antenna array elements. Both objective functions are normalized. The current optimization problem is multi-objective and non-convex, which we use CD framework to obtain a local solution for it.

B. Proposed method

The optimization problem in (4), will be solved out over two different stages: 1) w.r.t. α for fixed $\mathbf{P}_t$ and $\mathbf{P}_r$, which has a closed-form solution for the related quadratic convex optimization, with a minimizer below:

$$\alpha = \frac{vec(\mathbf{V}_d)^T vec(\mathbf{P}_t * \mathbf{P}_r)}{||vec(\mathbf{P}_t * \mathbf{P}_r)||^2} \tag{7}$$

and 2) w.r.t. $\mathbf{P}_t$ and $\mathbf{P}_r$ for a fixed α: $\mathbf{P}_t$ and $\mathbf{P}_r$ are binary matrices, so the problem with respect to these matrices is a discrete binary optimization problem. First, let us assume $\eta = 0$. To solve the problem, a CD approach is proposed, as described in Section II. Here, single variables of the CD approach are the positions of Tx and the Rx array elements. In each single variable optimization problem, for any entry of $\mathbf{P}_t$ and $\mathbf{P}_r$ ($t_{\tilde{i},\tilde{j}}$ and $r_{\bar{i},\bar{j}} \in \{0,1\}$), the minimizer to the problem will be kept in each iteration, while all the other elements are considered to be fixed. Then, the matrices $\mathbf{P}_t^i$ and $\mathbf{P}_r^i$ will be updated, subsequently. Here, $\mathbf{P}_t^i$ (or $\mathbf{P}_r^i$) is the updated Tx (or Rx) antenna array position matrix in the i-th iteration of the algorithm. This process will continue iteratively until the difference between two consecutive normalized objective functions is less than a pre-defined threshold.

Secondly, the above mentioned procedure will be repeated over a sequence of different values of scaling parameter $\eta \geqslant 0$. In the first step, where $\eta = 0$, a desired virtual array will be designed without considering the limitation on the number of Tx and Rx elements. Then, the output of the algorithm for $\eta = 0$ is considered as an input to the second iterative

algorithm for another value of η, e.g. $\eta = 0.1$. In this case, the second normalized objective function g_2 attempts to reduce the number of Tx/Rx elements, while g_1 maintains the desired virtual array. When $\eta \to 1$, the algorithm can achieve the predefined number of Tx/Rx elements such that they guarantee the desired virtual array. The proposed algorithm, **TALA**, is summarized in **Algorithm 2**.

Note that to efficiently implement the convolution in iterations of CD method, we use the distributive property of convolution, that is $x_1[.,.] * (x_2[.,.] + x_3[.,.]) = x_1[.,.] * x_2[.,.] + x_1[.,.] * x_3[.,.]$ and the Dirichlet function convolution property, $x[n,m] * \delta[n-n', m-m'] = x[n-n', m-m']$. In CD procedure, we calculate the convolution for every single variable, say each entry $(\bar{i}, \bar{j})$ of the Tx and Rx array antennas, for the two possible solutions in the binary set $\{0, 1\}$. To include this binary element change, we define $\Delta_{\bar{i}\bar{j}}$ as a matrix of size $\mathbf{P}_r$ with only a nonzero element in $(\bar{i}, \bar{j})^{th}$ position such that $\Delta_{\bar{i}\bar{j}}(\bar{i}, \bar{j}) = 1$. In this manner, we can write the new virtual array while updating $(\bar{i}, \bar{j})^{th}$ entry, $\mathbf{V}^{\kappa}_{\bar{i}\bar{j}}$ based on the previous updated virtual array, $\mathbf{V}^{\kappa-1}_{\bar{i}\bar{j}}$ as:

$$\begin{aligned}\mathbf{V}^{\kappa}_{\bar{i}\bar{j}} =& \mathbf{P}^{\kappa-1}_t * (\mathbf{P}^{\kappa-1}_r \pm \Delta_{\bar{i}\bar{j}}) = \mathbf{V}^{\kappa-1}_{\bar{i}\bar{j}} \pm (\mathbf{P}^{\kappa-1}_t * \Delta_{\bar{i}\bar{j}}) \\ =& \mathbf{V}^{\kappa-1}_{\bar{i}\bar{j}} \pm \mathbf{Z}_{\bar{i}\bar{j}}\end{aligned} \tag{8}$$

where $\pm$ is for two scenarios of placing and not placing an antenna element in the position $(\bar{i}, \bar{j})$. The matrix $\mathbf{Z}_{\bar{i}\bar{j}} \in \mathbb{R}^{(M_t+N_t-1)\times(M_r+N_r-1)}$ is a matrix of zero elements with only a non zero sub-matrix $\mathbf{P}^{\kappa-1}_r$ beginning from the $(\bar{i}, \bar{j})^{th}$ positions of the matrix $\mathbf{Z}_{\bar{i}\bar{j}}$. In this way, we can reduce the complexity of the large matrices convolution with only a simple summation operator and enhance the run time of the algorithm, significantly. Here, the equations are written for the case where CD method is applied to update Rx array position matrix. For the Tx one, we can rewrite the equations, similarly.

As we described earlier in Section I, in order to provide a good angular resolution, we need to increase the virtual aperture size, which is obtained by convolving the locations of transmitter and receiver elements. Hence, the properties of the virtual array are affected by the physical placement of transmitting and receiving elements. To have the maximum virtual aperture created and to be able to discriminate the signals emitted from different transmitters of the MIMO radar at the receiver, transmitted signals must be orthogonal [33]. In the sequel, we present our proposed waveform optimization to design a set of orthogonal code sequence for cognitive PMCW radars compatible to other communication systems in a coexistence scenario.

Algorithm 2 TALA: MIMO Vir**t**ual **A**rray Design A**l**gorithm for mmWave 4D-Imaging R**a**dar Sensors.

Inputs: Initialize random array elements positions ($\mathbf{P}^0_t$ and $\mathbf{P}^0_r$), $\alpha = 1$, predefined threshold value ϵ, a series of η values $\in [0, 1]$, the number of required Tx and Rx array elements L_T, and L_R, and input $\mathbf{V}_d$.
Outputs: $\mathbf{P}^\star_t$ and $\mathbf{P}^\star_r$ (Solutions of (4)).
$j \leftarrow 1$;
$i \leftarrow 0$;
Compute g^0_1 and g^0_2 from (5) and (6);
Compute $s(0) = g^0_1 + \eta(j) g^0_2$;
while $j \leq$ length(η) **do**
  for $i = 0, 1, 2, \ldots$ **do**
    $i \leftarrow i + 1$
    Update α^i using (7);
    Update $\mathbf{P}^i_t$ and $\mathbf{P}^i_r$ using CD;
    Compute $s(i) = g^i_1 + \eta(j) g^i_2$;
    Break for loop if $s(i-1) - s(i) < \epsilon$;
  end for
  $\mathbf{P}^\star_t = \mathbf{P}^i_t$ and $\mathbf{P}^\star_r = \mathbf{P}^i_r$.
  $j \leftarrow j + 1$
  Break if $||\mathbf{P}_t||_0 = L_T$ and $||\mathbf{P}_r||_0 = L_R$;
end while
Outputs: $\mathbf{P}^\star_t$ and $\mathbf{P}^\star_r$.

IV. Waveform Optimization

A. Problem Formulation

In this section, we design a set of unimodular sequences for PMCW radars based on jointly minimizing their auto- and cross-correlation levels and shaping their spectrum. The aim here is to reduce the auto- and cross-correlation sidelobes of a sequence set as much as possible in a ROI, which can be calculated in principle based on the radar system's maximum detection range; i.e., $K_{ROI} = \frac{2BR_{max}}{c}$, where K_{ROI} is the number of ROI samples, B is bandwidth, c is the speed of the light and R_{max} is the maximum detection range. This methodology is useful when the pulse duration is much greater than the round-trip delay, as in PMCW automotive radar applications.

Let us assume that $\mathbf{X} \in \mathbb{C}^{M\times K}$ is the set of transmitted sequences in baseband with M transmit antennas and K samples for each transmitter, and $x_{m,k} = e^{j\phi_{m,k}}$, the $(m,k)^{th}$ entry of $\mathbf{X}$, is the k^{th} sample of m^{th} antenna. WISL metric is defined as:

$$\sum_{m=1}^{M}\sum_{l=1}^{M}\sum_{k'=-K+1}^{K-1} |\alpha_{m,l}(k') r_{m,l}(k')|^2 - \textstyle\sum_{m=1}^{M} |\alpha_{m,m}(0) K|^2 \tag{9}$$

where $\alpha_{m,l}(k') \in [0,1],\ \forall k' \in \{-K+1, \ldots, K-1\}$ represents an arbitrary set of weights, $r_{m,l}(k') \triangleq (\mathbf{x}_m \circledast \mathbf{x}_l)_{k'} = \sum_{k'=1}^{K-1} x_{m,k'} x^*_{l,K-k'}$ is the cross-correlation between the m^{th}- and the l^{th}- antenna transmitting waveforms, that are $\mathbf{x}_m = [x_{m,1}, x_{m,2}, ..., x_{m,K}]^T$ and $\mathbf{x}_l = [x_{l,1}, x_{l,2}, ..., x_{l,K}]^T$, $m, l \in \{1, 2, ..., M\}$. If $m = l$, $r_{m,l}(.)$ represents the auto-correlation of the m^{th} transmitting signal. k' is one of the different $(2K-1)$ lags in cross-correlation computation. Please note that $\sum_{m=1}^{M} |\alpha_{m,m}(0)K|^2$ is the weighted energy of the waveform which is essentially the zero-lag of the auto-correlations. Since the signals are constant modulus, this term is a constant and can be eliminated in the objective function. Cross-correlation can be written using vectorizing and convolution operation by $\mathbf{r}_{m,l} = conv(\mathbf{x}_m, \mathbf{x}^{*r}_l)$. By re-writing the cross-correlation in the frequency domain ($\mathbf{r}_{m,l} = \mathbf{F}^{-1}(\mathbf{F}\bar{\mathbf{x}}_m \odot \mathbf{F}\bar{\mathbf{x}}^{*r}_l)$), we define the following optimization problem:

$$\begin{cases} \min\limits_{\mathbf{X}} \quad f(\mathbf{X}) \triangleq \sum\limits_{m=1}^{M}\sum\limits_{l=1}^{M} ||\mathbf{a}_1 \odot \mathbf{F}^{-1}(\mathbf{a}_2 \odot \mathbf{F}\bar{\mathbf{x}}_m \odot \mathbf{F}\bar{\mathbf{x}}^{*r}_l)||_2^2 \\ s.t. \quad x_{m,k} \in \mathcal{X}_\infty \quad \text{or} \quad \mathcal{X}_L \end{cases} \tag{10}$$

where, $\mathbf{F}$ and $\mathbf{F}^{-1}$ are $(2K-1)$ points Discrete Fourier Transform (DFT) and Inverse Discrete Fourier Transform (IDFT) matrices, respectively. $\bar{\mathbf{x}}$, here, is a zero-padding operation, i.e., $\bar{\mathbf{x}}_m \triangleq [\mathbf{x}_m^T, \quad \mathbf{0}_{K-1\times 1}^T]^T$ is the $(K-1)$ zero-padded vector of the m^{th} transmitting waveform. $\mathbf{x}^{*r}_l \triangleq [x^*_{(l,K)}, x^*_{(l,K-1)}, ..., x^*_{(l,1)}]^T$ is the sequence reverse for the l^{th} antenna. $\mathbf{a}_1$ and $\mathbf{a}_2$ are WISL and spectral weight vectors, respectively. ROI is defined by the non-zero elements of $\mathbf{a}_1$, and $\mathbf{a}_2$ determines the waveforms frequency spectrum stop-bands. The term $(\mathbf{a}_2 \odot \mathbf{F}\bar{\mathbf{x}}_m \odot \mathbf{F}\bar{\mathbf{x}}^{*r}_l)$ is a vector of length $(2K-1)$. $\mathcal{X}_\infty = \{e^{j\phi}|\phi \in \Omega_\infty\}$, $\Omega_\infty \triangleq (-\pi, \pi]$ and $\mathcal{X}_L = \{e^{j\phi}|\phi \in \Omega_L\}$, $\Omega_L \triangleq \{0, \frac{2\pi}{L} \ldots, \frac{2\pi(L-1)}{L}\}$ indicate the unimodular and discrete phase with L alphabet size sequences. Since the unimodular and discrete phase are equality constraints and they are not an affine set, the related optimization problem is a non-convex, multi-variable and NP-hard problem.

B. Proposed Method

1) *Continuous-phase constraint*: To solve the above optimization problem under the continuous-phase constraint, we use a CD approach and define an entry-based optimization framework to formulate the problem in terms of a series of single-variable optimization problems. This requires to find the critical points and obtains the global optimum solution in each step of the CD approach. To this end, we consider each entry of $\mathbf{X}$ as the only variable to our problem, while keeping the others fixed. Let $x^{(i)}_{m_0,k_0}$ ($m_0 \in \{1,2,...,M\}$ and $k_0 \in \{1,2,...,K\}$) be the only entry variable of the k_0^{th} sample of the m_0^{th} antenna to be optimized in the i^{th} iteration. Storing other entries of $\mathbf{X}$ in $\mathbf{X}^i_{-(m_0,k_0)}$ and keeping them fixed, we can formulate the objective function ($f(\mathbf{X})$) in terms of $x^i_{m_0,k_0}$ as (for notation simplicity, we omit the iteration number in the equations below):

$$\begin{aligned} &f(x_{m_0,k_0}, \mathbf{X}_{-(m_0,k_0)}) = \\ &\nu_{-2}(\mathbf{X}) x^{*^2}_{m_0,k_0} + \nu_{-1}(\mathbf{X}) x^*_{m_0,k_0} + \nu_0(\mathbf{X}) \\ &+ \nu_1(\mathbf{X}) x_{m_0,k_0} + \nu_2(\mathbf{X}) x^2_{m_0,k_0} \end{aligned} \tag{11}$$

where the coefficients ν_{-2}, ν_{-1}, ν_0, ν_1 and ν_2 are the complex-valued functions of $\mathbf{X}$ having different values for each entry (m_0, k_0) and can be calculated based on the formulas given in Appendix A. Note that, since the objective function $f(\mathbf{X})$ in Eq. 10 is real-valued, it can be shown and easily proved that $\nu_{-2} = \nu_2^*$ and $\nu_{-1} = \nu_1^*$.

Considering the coefficients as $\nu_h(\mathbf{X})$, $h \in \{-2,-1,0,1,2\}$ and re-writing the above equation based on the phases of each entry ϕ_{m_0,k_0} and the phase matrix $\mathbf{\Phi}_{-(m_0,k_0)}$, equivalently we have:

$$f(\phi_{m_0,k_0}, \mathbf{\Phi}_{-(m_0,k_0)}) = \sum_{h=-2}^{2} \nu_h(\mathbf{\Phi}) e^{jh\phi_{m_0,k_0}} \tag{12}$$

To minimize the objective function over Ω_∞ on each entry ϕ_{m_0,k_0}, and as f are differentiable functions for $\phi \in \Omega_\infty$, we can find the solution to the problem $\frac{df(\phi)}{d\phi} = \frac{d\sum_{h=-2}^{2} \nu_h e^{jh\phi}}{d\phi} = 0$. In this regard, the derivative of $f(\phi)$ can be obtained by:

$$f^{'}(\phi) = \sum_{h=-2}^{2} jh\nu_h e^{jh\phi_{m_0,k_0}} \tag{13}$$

Finding the roots of the derivative function $f^{'}(\phi)$ in Eq. 13, is equivalent to find the roots of $-je^{2j\phi}f^{'}(\phi) = -2\nu_{-2} - \nu_{-1}e^{j\phi} + 0 \times e^{2j\phi}\nu_1 e^{3j\phi} + 2\nu_2 e^{4j\phi}$, and subsequently, is equivalent to find the roots of the following 4 degree polynomial function, with some manipulations and variable change $z \triangleq e^{j\phi}$. Thus, we have,

$$\sum_{n=0}^{4} \rho_n z^n = 0 \tag{14}$$

where $\rho_4 = 2\nu_2$, $\rho_3 = \nu_1$, $\rho_2 = 0$, $\rho_1 = -\nu_{-1} = -\nu_1^*$ and $\rho_0 = -2\nu_{-2} = -2\nu_2^*$. Assume $z_n, \quad n = \{1,...,4\}$ are the roots of Eq. 14, the roots of $f^{'}(\phi) = 0$ are then equal to $\phi_n = -j\ln(z_n), \quad n = \{1,...,4\}$. Note that we only admit the real roots for ϕ. Hence, the global optimum solution for ϕ is obtained by:

$$\phi^\star_{m_0,k_0} = \arg\min_{\phi}\{f(\phi)|\phi \in \{\phi_n, n = \{1,...,4\}, \Im(\phi_n) = 0\} \tag{15}$$

Subsequently, the optimum solution for $x^i_{m_0,k_0}$ is ${x^\star}^i_{m_0,k_0} = e^{j\phi^\star_{m_0,k_0}}$ and the sequence set matrix $\mathbf{X}^{\star i}$ in each iteration is updated until the convergence criteria is met. The proposed CD algorithm for entry-based waveform optimization on the continuous-phase set is summerized in **Algorithm 2**.

Remark: Note that, since $f(\phi)$ in Eq. 12 is a function of $\sin\phi$ and $\cos\phi$, it is periodic, real and differentiable over $\Omega_\infty = (-\pi, \pi]$ and has at least two extrema and hence its derivative has at least two real roots. As a result, the feasibility of Eq. 15 in each iteration is guaranteed and the problem has the optimum solution.

2) *Discrete-phase constraint*: To solve the optimization problem (10) on a discrete-phase constraint $\Omega_L = \{\phi_0, \phi_1, \ldots, \phi_L\} \in \{0, \frac{2\pi}{L} \ldots, \frac{2\pi(L-1)}{L}\}$, with a finite alphabet size L, we use an exhaustive search method on all the critical points of the problem in Ω_L, for each entry x_{m_0,k_0} in the CD-based approach. Thus, to examine the optimum solution to the problem on Ω_L set, all the possible values of the objective function $f(\phi)$ is computed and the phase which minimizes the objective function is selected such that,

$$\phi^\star_{m_0,k_0} = \arg\min_{\phi}\{f(\phi)|\phi \in \Omega_L\} \tag{16}$$

Another way to optimize the problem considering the discrete-phase constraint is to use Fast Fourier Transform (FFT). It can be shown that $f(\phi)$ can be written with respect to alphabet indices ($l \in 1,2,...,L$) and the optimum solution is (see Appendix B for details):

$$l^\star = \arg\min_{l=1,...,L}\{f(l) = |\mathbf{F}^L\{\nu_2, \nu_1, \nu_0, \nu_1^*, \nu_2^*\}|\} \tag{17}$$

where $\mathbf{F}^L$ is L-point DFT operator. Hence, the corresponding optimum phase and waveform sample are $\phi^\star_{m_0,k_0} = \frac{2\pi(l^\star-1)}{L}$

Algorithm 3 Entry-Based Waveform Optimization on a Continuous (Ω_∞) or Discrete (Ω_L) Phase Set.

Inputs: Initialize random feasible set of sequences $\mathbf{X}^{(0)}$, predefined threshold value ϵ, $\mathbf{a}_1$ and $\mathbf{a}_2$ weight vectors. In case of discrete-phase design, Initialize alphabet size L and discrete-phase alphabet set Ω_L.
Outputs: $\mathbf{X}^\star$ (Solution of (10)).
$i \leftarrow 0$;
Compute $f(\mathbf{X}^{(0)})$ from (10);
for $i = 0, 1, ...$ **do**
$i \leftarrow i + 1$
  for $m_0 = 1, \ldots, M$ **do**
    for $k_0 = 1, \ldots, K$ **do**
      Calculate ν_1 and ν_2 using TABLE IV;
      if $x_{m_0,k_0} \in \mathcal{X}_\infty$ (Continous-Phase) **do**
        Calculate $\rho_n, \quad n = \{1, ..., 4\}$ in (14);
        Find the roots z_n from (14);
        Compute $\phi_n = -j \ln(z_n), \quad n = \{1, ..., 4\}$;
        Find the solution $\phi^\star_{m_0,k_0}$ to the problem (15);
      else $x_{m_0,k_0} \in \mathcal{X}_L$ (Discrete-Phase) **do**
        Calculate $f(l) = \mathbf{F}^L\{\nu_2, \nu_1, \nu_0, \nu_1^*, \nu_2^*\}$;
        Find l^* from (17);
        Compute $\phi^\star_{m_0,k_0} = \frac{2\pi(l^*-1)}{L}$;
      end if
      Update $x^i_{m_0,k_0} = e^{j\phi^\star_{m_0,k_0}}$;
      $\mathbf{X}^i = \mathbf{X}^i_{-(m_0,k_0)}|_{x_{m_0,k_0}=x^i_{m_0,k_0}}$;
    end for
  end for
Compute $f(\mathbf{X}^i)$ from (10);
Stop if $[f(\mathbf{X}^i) - f(\mathbf{X}^{i-1})]/||f(\mathbf{X}^i)||_F > \epsilon$
end for
Outputs: $\mathbf{X}^\star = \mathbf{X}^i$.

and $x^{\star i}_{m_0,k_0} = e^{j\phi^\star_{m_0,k_0}}$, respectively. In these two methods for discrete-phase constraint, the computational complexity of the problem grows up with increasing the alphabet size L.

V. Simulation and Results

In this section, we provide numerical examples in order to assess the performance of the proposed algorithms in both MIMO virtual Array design problem in Section III and waveform optimization in Section IV.

A. MIMO Virtual Array Design Problem

In order to validate the proposed method discussed in this paper for the virtual array design problem, we first consider a virtual array of some Commercial Off-The-Shelf (COTS) as the desired virtual array, and then set the number of Tx/Rx antennas equal to the ones already considered for the COTS. In this case, we anticipate mimicking the virtual array of the COTS, but not necessarily with identical Tx/Rx physical configurations. This gives chip designers additional insight on the placement of Tx/Rx antenna elements while still satisfying the same virtual array. Furthermore, given different initializations for $\mathbf{P}_t^0$ and $\mathbf{P}_r^0$ in **Algorithm 2**, a new configuration for Tx/Rx antenna elements can be obtained, expanding the design possibilities for chip designers in practical applications.

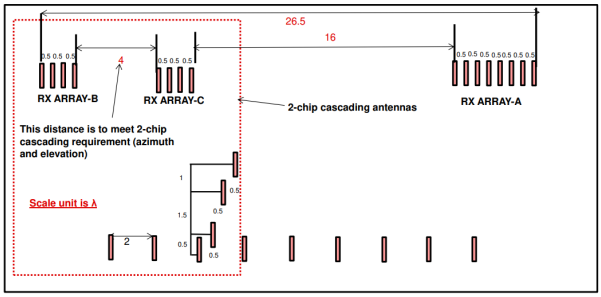

Fig. 1: Antenna Array Positions. Image taken from [63]

In addition, we can show how to construct an arbitrary virtual array, which may or may not be feasible given the number of physical Tx/Rx antenna elements. It would be possible to demonstrate that using the proposed framework, the design procedure can be close to the desired virtual array configuration while satisfying the number of Tx/Rx antenna elements.

Example 1: In the first example, we consider TI imaging radar (from Texas Instruments), with $L_T = 12$ Tx and $L_R = 16$ Rx channels. The Tx/Rx antenna array positions are based on AWR2243 cascade 4D-Imaging radar (see Fig. 1) [63]. In our problem, we consider the virtual array of this configuration as the desired one ($\mathbf{V_d}$), with $M_t = 64$ and $N_t = 12$, and also $M_r = 64$ and $N_r = 1$ separated grid points in a coordinate plane with a half-wavelength inter-grid interval, i.e. $d = \lambda/2$ that can be applied to place antennas. Using an increasing scheme for η values as described for **Algorithm 2**, we examine the convergence behaviour of the proposed method in Fig. 2a. We set $\epsilon = 10^{-5}$ in all of our simulations. It can be seen that, the normalized objective function of the optimization problem in (4) has a monotonically decreasing cost function value. This is due to the nature of CD method, which guarantees a decrement in the objective values. The desired and the designed MIMO virtual array are also depicted in Fig. 2b. The obtained locations of the Tx/Rx antenna elements on a grid-point 2D planar array, which lead to the designed virtual array, are shown in Fig. 2c, which corresponds to the antenna array positions in [63] and confirms the proposed algorithm.

Note that running the algorithm multiple times and using different settings can result in diverse outcomes for the Tx/Rx array configuration as it converges to various local optimum solutions. As previously mentioned, the array's design and implementation can be customized to adhere to specific physical constraints, including the dimensions of the Tx/Rx array necessary for module construction. In Example 1, we showcase the results that closely resemble the TI-array structure, effectively demonstrating how our proposed algorithm mimics the behavior of an off-the-shelf component.

Example 2: The used radar system platform, as a second case study, has been described in [3]. Here, a MIMO array with $L_T = 4$ and $L_R = 16$ has been used. We applied this setting to our proposed design method with $M_t = 16$, $N_t = 48$, $M_r = 16$, and $N_r = 32$. The objective function is depicted in

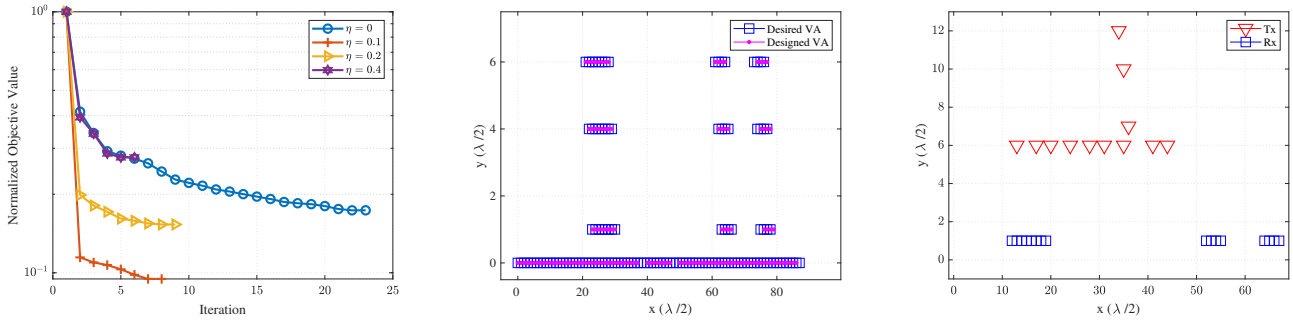

(a) (b) (c)

Fig. 2: **Example 1** [63]: (a) Convergence curve of the proposed algorithm for different η values. (b) Dense configuration of designed and desired virtual array (VA).

(c) Obtained Tx/Rx antenna positions.

Fig. 3a. Fig. 3b demonstrates the desired and designed MIMO virtual array. The obtained Tx/Rx array configuration is also depicted in Fig. 3c confirming the design described in [3].

Example 3: An advanced 4D-Imaging radar-on-chip developed by Vayyar [64] has been used as a case study. The chip includes an integrated Digital Signal Processor (DSP), Micro Controller Unit (MCU), and up to 48 transceivers for real-time signal processing that provides an ultra-wide field of view and exceptional resolution with a single chip. In this case, the desired and designed virtual array can be seen in Fig. 5a. The designed virtual array for $L_T = L_R = 24$ has been obtained with $M_t = N_t = M_r = N_r = 24$ and the proposed algorithm converged with the scaling factor (η) equals to 0. The results for the array configuration is shown in Fig. 5d.

Example 4: A MIMO radar architecture, based on 24 Tx and 24 Rx array elements working in the frequency range between 16 and 17 GHz has been proposed in [65] as a complete 3D imaging FMCW MIMO radar implemented by TDM of the transmit signals. Tx/Rx elements are placed forming a rectangle which can be seen in Fig. 4 with the angular resolution of 2.5 degree. To reduce the coupling between radiating elements and to increase the angular resolution, the distance between antennas was chosen to be greater than $\lambda/2$ which is equal to 9.7 mm in this radar system setting. To handle the grating lobes appear in this manner, the elements are placed with the distances equal to 15 mm such that the grating lobes be outside of the desired FoV. with this form, an improvement of near 10 dB in the coupling is achieved in comparison with 9.7 mm distance. The front view of the antenna array is shown in Fig. 4 and the related virtual array, considered as a desired one in our algorithm, is depicted in Fig. 5b. In order to apply this array setting to our method, we set $L_T = L_R = 24$, $M_t = M_r = 12$, $N_t = N_r = 24$. The resulting virtual array and array configuration is demonstrated in Fig. 5b and Fig. 5e.

Example 5: In the next example, we consider the designed virtual array in [11] as the desired one in our algorithm, that is shown in Fig. 5c. This virtual array is the sparse form of the 3D-Imaging radar virtual array developed by Vayyar, Walabot-60GHz with 40 transmitter and receiver Radio Frequency (Rf) channels, with 20 Tx and 20 Rx linearly polarized wide-band antennas over the frequency band of 62 to 63.6 GHz. The conventional topology of both Tx/Rx array by Vayyar is regular dense with an element spacing of $\lambda/2$ at 64 GHz placed in orthogonal directions. The virtual antenna array is then a 2D MIMO virtual array with regular dense spacing. To achieve a narrower beam-width and lower side-lobe level as compared to a dense array, sparse Tx, sparse Rx, and ultimately sparse virtual array is introduced in [11]. The peak Side-lobe level is 7 dB lower and the beam-width is improved by about 2 degree with this sparse-array arrangement. The resultant sparse array configuration of our algorithm for this desired virtual array elements with $L_T = L_R = 20$, $M_t = 200$, $M_r = 5$, $N_t = 1$, $N_r = 200$ can be seen in Fig. 5f. The designed virtual array matches the desired one which is depicted in Fig. 5c.

Example 6: In this example, a 79 GHz high-resolution 4D-Imaging MIMO radar with 1728 virtual channels proposed in [7] is considered as the other case study. The proposed radar system is composed of 12 transceiver MMICs, each one contains 3 Tx and 4 Rx channels. A configuration of a 6×2 MMICs array to enlarge the aperture in azimuth and elevation direction is shown in Fig. 6. The antennas are placed in a 2 mm grid points in azimuth (a slightly larger than $\lambda/2$) and 2.5 mm in elevation. To enable transmit beamforming, each of the 6 transmit antennas is grouped as a 2×3 URA configuration. The dense representation of the virtual array of this configuration is shown in Fig. 7a, with $L_T = 36$ Tx and $L_R = 48$ Rx antenna elements, which is obtained by setting $M_t = 95$, $M_r = 20$, $N_t = 99$, $N_r = 25$. The resulting 2D array configuration is also depicted in Fig. 7b.

In TABLE I, we compare the obtained virtual array of different case studies when their virtual array was used as the desired one. This table shows the number of Tx/Rx obtained in each step of the algorithm regarding different values of η. The process follows **Algorithm 2**, where initially the entire problem is solved using the CD approach for $\eta = 0$. The solution from this step serves as input for the next iteration with $\eta = 0.1$. This process continues for other values of η within the range of $[0, 0.1, ..., 1]$ until the termination condition specified in line 17 of the algorithm is satisfied. If the algorithm stops for a specific value of η, it indicates that the desired number of Tx and Rx elements has already been

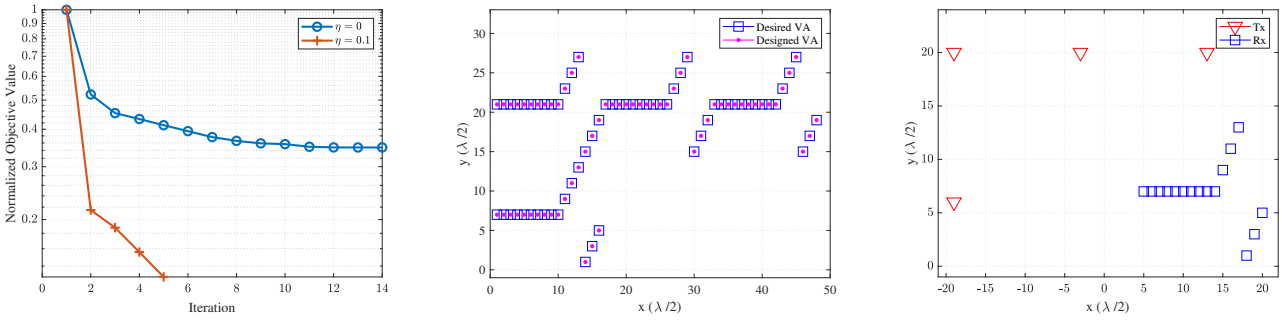

(a) (b) (c)

Fig. 3: **Example 2** [3]: (a) Convergence curve of the proposed algorithm for different η values. (b) Dense configuration of designed and desired virtual array (VA). (c) Obtained Tx/Rx antenna positions.

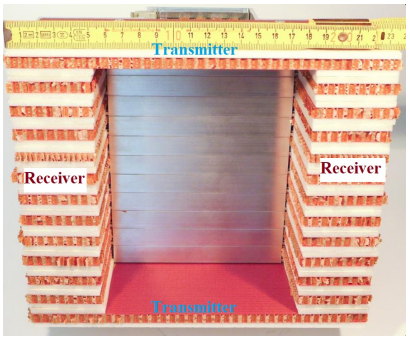

Fig. 4: Front view of Tx/Rx antenna array proposed in [65].

obtained before progressing to the next η value. Therefore, in the table, we represent such cases with a "-". The results in the table demonstrate that depending on the chosen settings and examples, the algorithm may converge either for $\eta = 0$ or after multiple iterations over different η values. By doing so, the proposed algorithm successfully emulates the desired virtual array as presented in different examples.

Finally in Fig. 8, we show that the algorithm is able to mimic an arbitrary virtual array, which is a circular array in this example. We consider our design with $L_T = 23$ and $L_R = 16$, and set $M_t = N_t = 23$ and $M_r = N_r = 5$.

B. Waveform Design

In this section, we provide numerical examples and simulation results to assess the performance of our proposed waveform for PMCW radars.

The ISL values of the designed waveforms are given in Table II. In this table, to compare the proposed method with others for only ISL minimization, we consider $K = 64$, and we set all elements of the weight vectors $\mathbf{a}_1$ and $\mathbf{a}_2$ equal to 1. This table shows the comparison between the ISL values of a set of random-phase sequences with Multi-CAN [49], MM-Corr [52] BiST [30], and the proposed method in this paper when we do not consider any ROI (i. e., $K_{ROI} = K$). Note that, the difference between the ISL values of a set of random-phase codes and the lower bound is less than 0.5 dB when $M = 10$ for a set of sequences with $N = 64$. This small difference in ISL values is not enough to design a set of orthogonal code sequences in a massive MIMO radar system [57] such as 4D-imaging radar sensors.

On the other hand, Table III shows the impact of considering ROI in the proposed waveform optimization framework. As discussed above, Table II solely compares the ISL values obtained using various state-of-the-art methods, highlighting that minimizing ISL alone does not guarantee a set of good orthogonal sequences for PMCW radars. However, when taking into account the defined ROI in our design, as shown in Table III, the resulting sequence set is capable of achieving remarkably low sidelobe levels in the maximum range of the radar. This table provides the ISL values for different number of antennas and different code lengths and shows that, according to a required code length, the proposed waveform optimization can achieve very low-sidelobe levels in the required range gates by increasing the ratio $\frac{K}{K_{ROI}}$. Although in our proposed waveform design approach the auto- and cross-correlation functions have very high sidelobe levels outside of ROI ($[-K+1, -K_{ROI}-1] \cup [K_{ROI}+1, K-1]$), only the sidelobe levels in the ROI determine the performance of the radar system and we can perfectly use it in automotive applications due to the small required ROI.

To compare the impact of different parameters of our proposed waveform design in terms of auto-correlation properties, Fig. 9 represents the auto-correlation functions (dB-values) of the second transmit antenna code sequence for different settings of code lengths, ROI lengths, number of antennas, and spectrum-nulling. It is evident that, as we expected, with an increase in the number of transmit antennas and nulling the stop-bands the auto-correlation functions become worse, yet by considering the ROI and with increasing the ratio $\frac{K}{K_{ROI}}$, we can achieve low sidelobe levels in the auto-correlation functions, while shaping the spectrum as well. The corresponding auto-correlation functions, for the same setting, have also been depicted in this figure for the discrete phase code set with the number of $L = 16$ discrete phases. As it is evident, continuous-phase code set design can achieve the lower sidelobe levels, due to finding the global optimum solutions in each step of CD approach, through the proposed algorithm. However, using the discrete-phase sequences result in a substantial reduction in hardware implementation complexity.

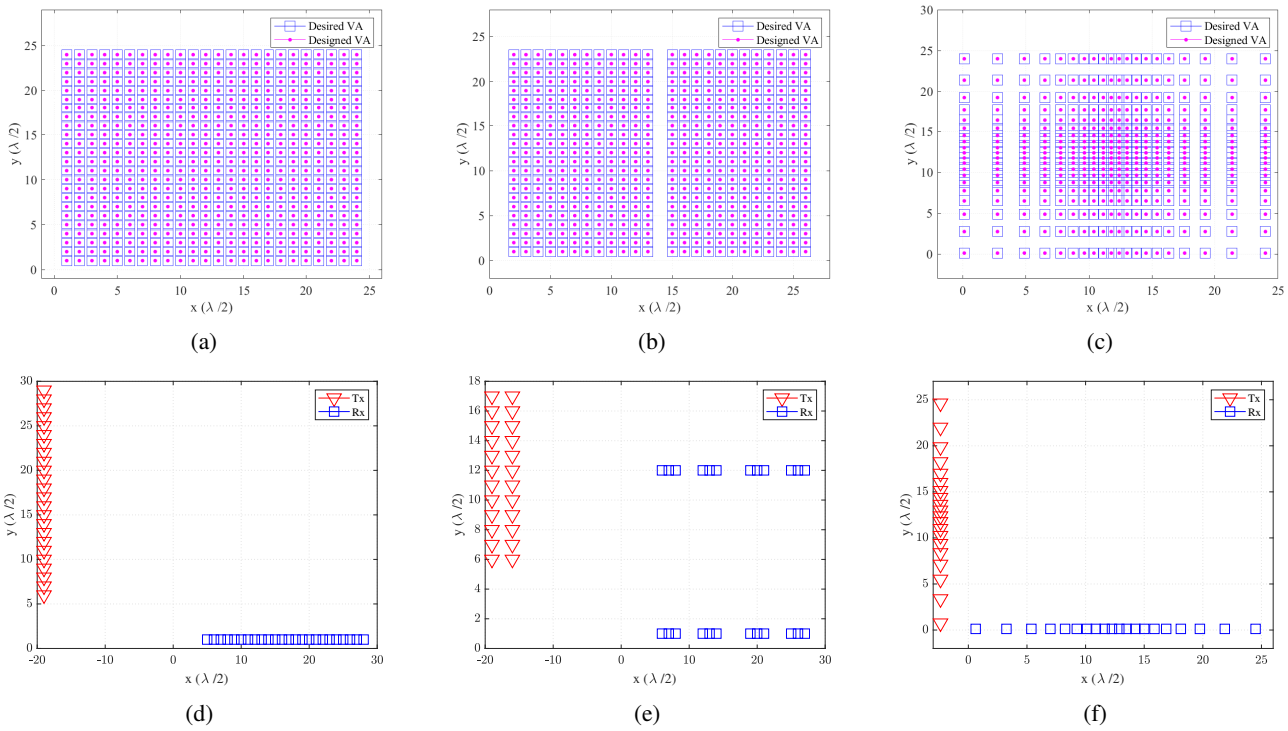

Fig. 5: Upper row: Dense configuration of designed and desired virtual array (VA) for (a) **Example 3** [64], (b) **Example 4** [65] and (c) **Example 5** [11], and Bottom row: Obtained Tx/Rx antenna positions for the same examples as (a)-(c), respectively.

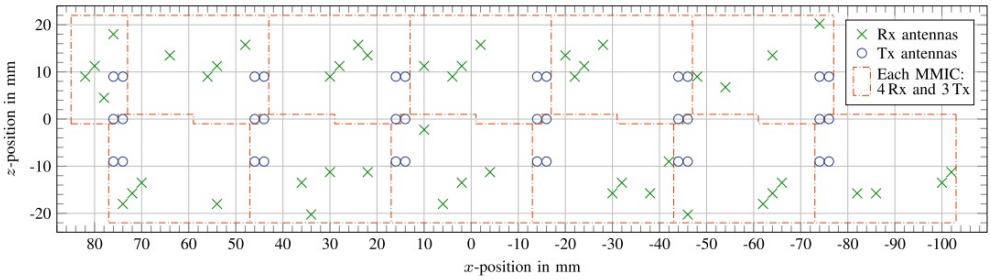

Fig. 6: Proposed Tx/Rx antenna array positions in [7].

TABLE I: The number of transmitter and receiver obtained in each step of the proposed algorithm for different values of η.

Scaling Factor	**[63]**		**[3]**		**[64]**		**[65]**		**[11]**		**[66]**		**[7]**	
	L_T	L_R	L_T	L_R	L_T	L_R	L_T	L_R	L_T	L_R	L_T	L_R	L_T	L_R
$\eta = 0$	40	23	28	17	24	24	25	52	20	20	86	19	36	190
$\eta = 0.1$	24	18	4	16	-	-	25	45	-	-	24	18	36	48
$\eta = 0.2$	13	16	-	-	-	-	24	24	-	-	23	16	-	-
$\eta = 0.4$	12	16	-	-	-	-	-	-	-	-	-	-	-	-

Fig. 10 shows the convergence curve of the CD approach for different settings such as code lengths, ROI samples, the number of antennas and the alphabet size (for discrete-phase design in Fig. 10b) in the proposed **Algorithm 3** for entry-based waveform optimization. The figure shows the monotonically decreasing objective values for different waveforms.

Furthermore, in order to compare the range sidelobe level of our proposed method with other traditional waveforms such as FMCW and Golomb sequence at the receive side, we show the range profile of each waveform in Fig. 11a. In this example, we set $B = 200$MHz, $K = 2000$ samples and $R_{max} = 50$ m ($K_{ROI} = 100$ samples). We assume two targets are located in the range of 15 and 25 m, respectively. This figure shows that our proposed waveforms (for $M = 2$, $M = 12$, and even $M = 12$ with spectrum shaping for continuous-phase design) have a lower sidelobe levels (in the ROI) while maintaining almost the same mainlobe width. This figure, also, shows the result for discrete-phase design with $M = 2$ and $L = 16$. Note that, in this figure, the range profile of our proposed method for each setting ($M = 2$, $M = 12$, and $M = 12$ with spectrum shaping) is the mean of all antennas matched-filter outputs. Further, the chirp signal in FMCW and Golomb

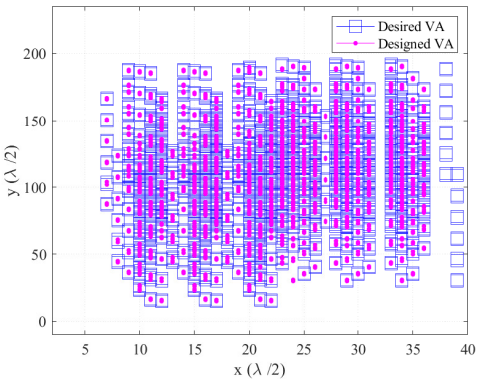

(a)

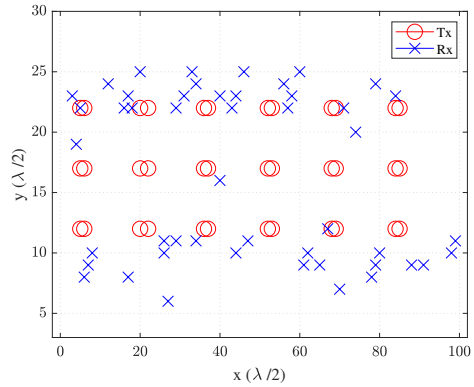

(b)

Fig. 7: a): Dense configuration of designed and desired virtual array (VA) [5] and b): Obtained Tx/Rx antenna positions.

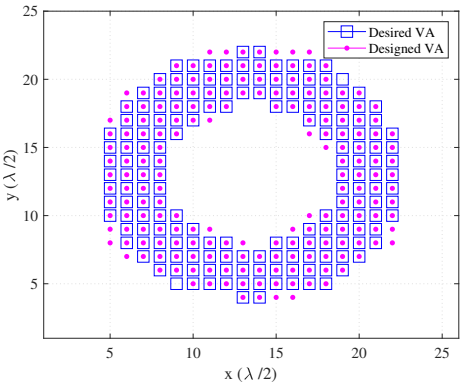

(a)

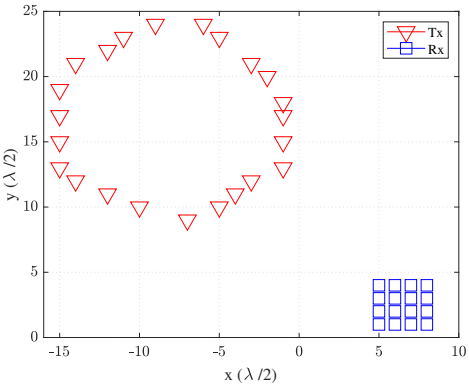

(b)

Fig. 8: a): Dense configuration of designed and desired virtual array (VA) and b): Obtained Tx/Rx antenna positions.

sequence are assumed to be transmitted from a single antenna herein. Hence, in the case of using multiplexing techniques for MIMO FMCW radars or transmitting any other MIMO PMCW sequences lead to a decrease in the performance of radars compared to that of single input FMCW and Golomb sequence in Fig. 11a. This shows that our proposed method have the capability to outperform other methods in the MIMO scenario. Fig. 11b illustrates the range profile of the PMCW waveforms (random-phase and proposed waveforms) with $M = 2$ and the total of $K = 2000$ samples. It can be seen that, by considering the weights $\alpha_k = 1$, $k \in \{-1999, \ldots, 1999\}$ (when ROI equals to the code length ($K = K_{ROI} = 2000$)), our proposed method has almost the same performance as the random-phase sequence. On the other hand, an optimized set of sequences with weights in the ROI (corresponding to $K_{ROI} = 100$ samples), significantly reduces the range sidelobes, and outperforms the others.

For the spectrum nulling in the undesired stop-bands, we consider two scenarios for two different code lengths for continuous-phase code set design and also we consider discrete-phase design with $L = 16$ in Fig. 12a in which $K_{ROI} = 100$. To compare the obtained results with [57], we set $M = 2$ and the stop-bands based on the normalized frequency are $[0.3, 0.35] \cup [0.7, 0.8]$ for the code length of 256 and 512. Although the depth of the nulls in our proposed method is not as good as [57], we achieved better ISL due to the ROI consideration. This figure shows that the proposed method can design a set of spectrally compatible code sequences with good properties in terms of ISL, while imposing nulls in undesirable stop-bands. Further, we compared the spectrum of our proposed waveforms with [58], which designs spectrally compatible waveforms for beampattern formation. Fig. 12b shows better results for our proposed method. In this figure, to compare our results with [58], we set $K = 512$, $K_{ROI} = 200$, equal to the code lengths in [58], $M = 50$, and $[0.25, 0.5]$ for the normalized frequency of an undesired stop-band in designing both continuous- and discrete-phase (with $L = 32$) set of sequences.

VI. Conclusion

In this paper, the problem of designing a desired virtual array and the Tx/Rx antenna positions to approximate the virtual array with a particular number of array elements was studied, applicable for 4D-Imaging automotive radar sensors. In order to tackle the problem, we proposed a sequence of iterative algorithms based on CD method. Numerical examples were provided demonstrating the excellent performance of the proposed method for obtaining arbitrary configurations of different virtual arrays. To design orthogonal transmit waveforms, we consider CDM-MIMO for PMCW radars in spectrally crowded environments and we proposed an entry-based optimization method to jointly design constant modulus

TABLE II: Comparison between the ISL (dB)-values of different sequences and random-phase sequences ($K = 64$).

M	2	3	4	5	6	7	8	9	10
Random-phase	5.9289	9.8565	11.9106	14.0384	15.5558	16.8349	18.0590	19.2051	19.9744
Multi-CAN [49]	3.0103	7.7815	10.7918	13.0103	14.7712	16.2325	17.4819	18.5733	19.5424
MM-Corr [52]	3.0103	7.7815	10.7918	13.0103	14.7712	16.2325	17.4819	18.5733	19.5424
BiST [30] ($\theta = 0$, $L = 8$)	3.2632	7.8529	10.8238	13.0302	14.7901	16.2411	17.4884	18.5796	19.5458
Proposed method ($K_{ROI} = 64, K = 64$)	3.1487	7.8052	10.7975	13.0142	14.7773	16.2346	17.4837	18.5745	19.5433
Lower bound	3.0103	7.7815	10.7918	13.0103	14.7712	16.2325	17.4819	18.5733	19.5424

TABLE III: Comparison between the ISL (dB)-values of the proposed method for different code lengths ($K_{ROI} = 64$).

M	2	3	4	5	6	7	8	9	10
$K = 128$	-13.4972	-4.2372	2.2743	5.4578	7.9316	9.7548	11.3160	12.6290	13.7356
$K = 256$	-25.1622	-17.8270	-10.6694	-5.7151	-1.2017	2.6200	5.1869	7.0659	8.7133
$K = 512$	-33.8273	-29.5091	-23.3246	-17.6190	-15.4697	-10.4416	-7.9380	-5.7282	-2.7758
$K = 1024$	-40.9693	-36.2091	-30.4133	-30.6181	-27.3662	-24.1144	-20.3935	-17.2538	-14.1951

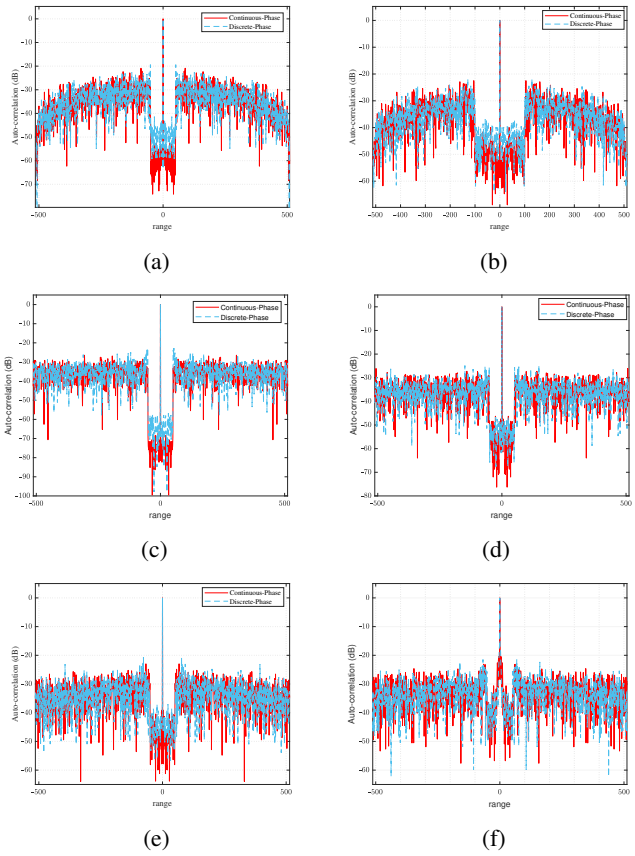

Fig. 9: Auto-correlation functions for (a) $K = 512$, $K_{ROI} = 100$, $M = 2$, and no stop-bands, (b) $K = 512$, $K_{ROI} = 200$, $M = 2$, and no stop-bands, (c) $K = 2000$, $K_{ROI} = 100$, $M = 2$, and no stop-bands, (d) $K = 2000$, $K_{ROI} = 100$, $M = 12$, and no stop-bands, (e) $K = 1024$, $K_{ROI} = 100$, $M = 12$, and no stop-bands, (f) $K = 1024$, $K_{ROI} = 100$, $M = 12$, and stop-bands. For discrete-phase code design, we considered the alphabet size of $L = 16$.

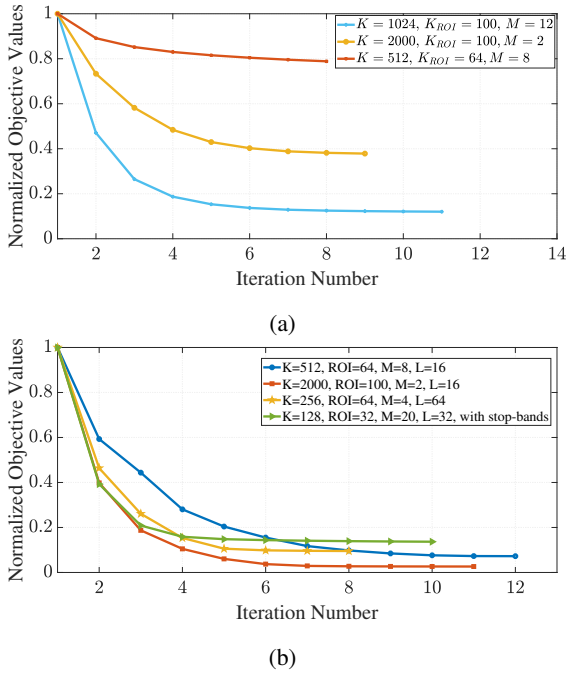

Fig. 10: (a) objective values of the proposed **Algorithm 3** for continuous-phase and (b) discrete-phase waveform design.

TABLE IV: Calculation of coefficients (ν_0,ν_1,ν_2) in Eq. 11.

ν_0	$f(\mathbf{X})\vert_{x_{m_0,k_0}=0}$ (10)
ν_1	$\sum_{\substack{m=1 \\ m\neq m_0}}^{M} [x^*_{m,k_0}\boldsymbol{\Upsilon}_0^H\boldsymbol{\Upsilon}_3(m,m_0) + x_{m,k_0}\boldsymbol{\Upsilon}_1^H(m_0)\boldsymbol{\Upsilon}_2(m) + \boldsymbol{\Upsilon}_1^H(m_0)\boldsymbol{\Upsilon}_3(m_0,m) + x_{m,k_0}\boldsymbol{\Upsilon}_1^H(m_0)\boldsymbol{\Upsilon}_2(m) + \boldsymbol{\Upsilon}_3^H(m_0,m)\boldsymbol{\Upsilon}_2(m) + x^*_{m,k_0}\boldsymbol{\Upsilon}_3^H(m_0,m)\boldsymbol{\Upsilon}_0]$ $+\boldsymbol{\Upsilon}_3^H(m_0,m_0)\boldsymbol{\Upsilon}_2(m_0) + \boldsymbol{\Upsilon}_1^H(m_0)\boldsymbol{\Upsilon}_3(m_0,m_0) + M\boldsymbol{\Upsilon}_1^H(m_0)\boldsymbol{\Upsilon}_0 + M\boldsymbol{\Upsilon}_0^H\boldsymbol{\Upsilon}_2(m_0)$
ν_2	$\boldsymbol{\Upsilon}_1^H(m_0)\boldsymbol{\Upsilon}_2(m_0)$

transmit sequences with near perfect orthogonality in terms of correlation sidelobes in the required ROI and spectrum shaping with defining an unconstrained optimization problem. We simulated and compared the performance of our proposed waveform design method and showed that our proposed waveforms can achieve a good performance in 4D-imaging automotive MIMO radar systems.

APPENDIX A

The objective function $f(\mathbf{X})$ in Eq. 10 can be written according to each entry of matrix $\mathbf{X}$ as a form of Eq. 11. In this form, the coefficients can be calculated from TABLE IV, where the parameters are defined as follows; $\mathbf{f}_{k_0}$ is a vector derived from the DFT matrix ($\mathbf{F}$) containing its k_0^{th} column elements. Similarly, $\mathbf{f}_{K+1-k_0}$ is the $(K+1-k_0)^{th}$ column of

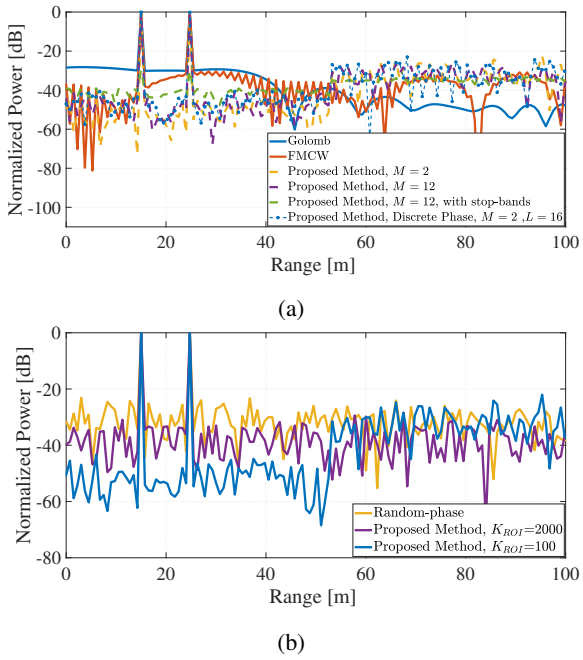

Fig. 11: (a) Range profile for FMCW and PMCW radar, and (b) Range profile for PMCW MIMO radar (random-phase sequences and proposed method.

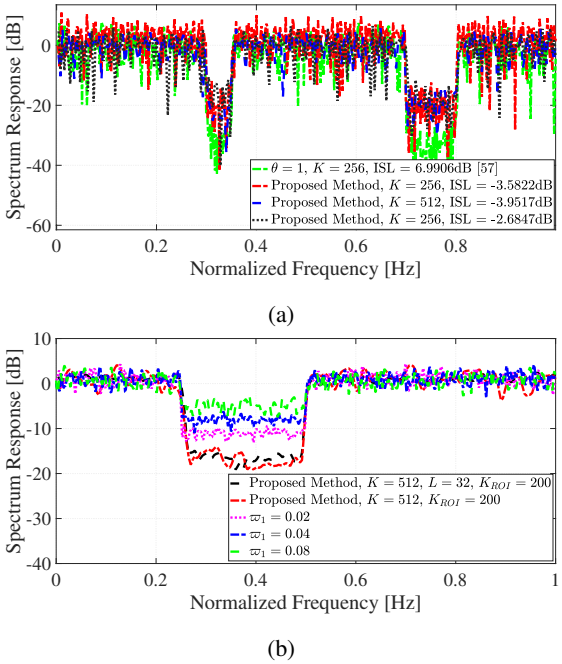

Fig. 12: (a) Spectrum of the proposed method for different code lengths and that of the method in [57] and (b) Spectrum of the proposed method compared to [58].

the matrix $\mathbf{F}$. Moreover, $\hat{\mathbf{F}}_{-k_0}$ is a $((2K-1)\times K)$ sub-matrix of $\mathbf{F}$ containing all first K columns of $\mathbf{F}$, except for the k_0^{th} column, i.e., in $\hat{\mathbf{F}}_{-k_0}$, the k_0^{th} column of $(\mathbf{F})$ is omitted. The same as $\hat{\mathbf{F}}_{-k_0}$, $\hat{\mathbf{F}}_{-K+1-k_0}$ is a sub-matrix of $\mathbf{F}$ in which the $(K+1-k_0)^{th}$ column is removed. Also, $\mathbf{x}_{m_0,k\neq k_0}$ is m_0^{th} antenna waveform (the m_0^{th} row of $\mathbf{X}$, in which the the k_0^{th} sample is dropped out and x_{m,k_0} is the k_0^{th} sample of m^{th} antenna waveform ($m \in \{1,2,...,M\}$). For simplifying the notations in TABLE IV, we define some auxiliary variables as,

$$\begin{cases} \boldsymbol{\Upsilon}_0 \triangleq \mathbf{a}_1^T \odot \mathbf{F}^{-1}(\mathbf{a}_2^T \odot \mathbf{f}_{k_0} \odot \mathbf{f}_{K+1-k_0}), \\ \boldsymbol{\Upsilon}_1(\hat{m}) \triangleq \mathbf{a}_1^T \odot \mathbf{F}^{-1}(\mathbf{a}_2^T \odot \hat{\mathbf{F}}_{-k_0}\mathbf{x}^T_{\hat{m},k\neq k_0} \odot \mathbf{f}_{K+1-k_0}), \\ \boldsymbol{\Upsilon}_2(\hat{m}) \triangleq \mathbf{a}_1^T \odot \mathbf{F}^{-1}(\mathbf{a}_2^T \odot \mathbf{f}_{k_0} \odot \hat{\mathbf{F}}_{-K+1-k_0}\mathbf{x}^{rH}_{\hat{m},k\neq k_0}), \\ \boldsymbol{\Upsilon}_3(\hat{m},\tilde{m}) \triangleq \mathbf{a}_1^T \odot \mathbf{F}^{-1}(\mathbf{a}_2^T \odot \hat{\mathbf{F}}_{-k_0}\mathbf{x}^T_{\hat{m},k\neq k_0} \odot \hat{\mathbf{F}}_{-K+1-k_0}\mathbf{x}^{rH}_{\tilde{m},k\neq k_0}). \end{cases} \tag{18}$$

where all of these auxiliary variables are vectors of length $(2K-1)$. Note that, for calculating ν_0, it can be proved that it is equivalent to computing the objective function in (10) considering $x_{m_0,k_0} = 0$, i.e., $f(\mathbf{X})|_{x_{m_0,k_0}=0}$.

To decrease the computational complexity of coefficients, we can implement them using FFT. To this end, it can be easily proved that $\hat{\mathbf{F}}_{-k_0}\mathbf{x}^T_{m,k\neq k_0}$ =FFT$\{\bar{\mathbf{x}}^T_m\} - x_{m,k_0}\mathbf{f}_{k_0}$. Similarly, we have, $\hat{\mathbf{F}}_{-K+1-k_0}\mathbf{x}^{rH}_{m,k\neq k_0}$ =FFT$\{\bar{\mathbf{x}}^{rH}_m\} - x^*_{m,K+1-k_0}\mathbf{f}_{K+1-k_0}$ and the same strategy can be adopted for other similar parameters in TABLE IV.

Note that, $\nu_{-2} = \nu_2^*$ and $\nu_{-1} = \nu_1^*$.

APPENDIX B

To solve the entry-based optimization problem (10) under discrete-phase constraint, since the phases are selected from a finite alphabet Ω_L, the objective function can be written as a function of indices of Ω_L as follows using Eq. 12,

$$e^{-2j\phi}f(\phi) = \nu_2 + \nu_1 e^{-j\phi} + \nu_0 e^{-2j\phi} + \nu_{-1}e^{-3j\phi} + \nu_{-2}e^{-4j\phi} \tag{19}$$

As $\phi \in \Omega_L = \{\phi_0, \phi_1, \ldots, \phi_L\} \in \{0, \frac{2\pi}{L} \ldots, \frac{2\pi(L-1)}{L}\}$, $e^{-2j\phi}f(\phi)$ follows the definition of L-point DFT of sequence $\{\nu_2, \nu_1, \nu_0, \nu_1^*, \nu_2^*\}$.

Note that, since the objective function $f(\phi)$ is real-and positive-valued ($f(\phi) = |f(\phi)|$) and minimizing the objective function is equivalent to minimizing its absolute value $|f(\phi)| = |e^{-2j\phi}f(\phi)|$, we can minimize $|e^{-2j\phi}f(\phi)|$ instead of $f(\phi)$.

REFERENCES

[1] J. Wenger, "Automotive mm-wave radar: Status and trends in system design and technology," 1998.

[2] I. Bilik, O. Longman, S. Villeval, and J. Tabrikian, "The rise of radar for autonomous vehicles: Signal processing solutions and future research directions," *IEEE Signal Processing Magazine*, vol. 36, no. 5, pp. 20–31, 2019.

[3] M. Stolz, M. Wolf, F. Meinl, M. Kunert, and W. Menzel, "A new antenna array and signal processing concept for an automotive 4D radar," in *2018 15th European Radar Conference (EuRAD)*, 2018, pp. 63–66.

[4] F. Roos, J. Bechter, C. Knill, B. Schweizer, and C. Waldschmidt, "Radar sensors for autonomous driving: Modulation schemes and interference mitigation," *IEEE Microwave Magazine*, vol. 20, pp. 58–72, 09 2019.

[5] D. Schwarz, C. Meyer, A. Dürr, A. Mushtaq, W. Winkler, and C. Waldschmidt, "System performance of a scalable 79 GHz Imaging MIMO Radar with injection-locked lo feedthrough," *IEEE Journal of Microwaves*, vol. 1, no. 4, pp. 941–949, 2021.

[6] I. Bekkerman and J. Tabrikian, "Target detection and localization using MIMO radars and sonars," *IEEE Trans. Signal Process.*, vol. 54, no. 10, pp. 3873–3883, 2006.

[7] D. Schwarz, N. Riese, I. Dorsch, and C. Waldschmidt, "System performance of a 79 ghz high-resolution 4d imaging mimo radar with 1728 virtual channels," *IEEE Journal of Microwaves*, vol. 2, no. 4, pp. 637–647, 2022.

[8] J. Bergin and J. R. Guerci, *MIMO Radar: Theory and Application*. Artech House, 2018.

[9] Z. Peng and C. Li, "A portable k -band 3-D MIMO radar with nonuniformly spaced array for short-range localization," *IEEE Transactions on Microwave Theory and Techniques*, vol. 66, no. 11, pp. 5075–5086, 2018.

[10] M. Deng, Z. Cheng, and Z. He, "Co-design of waveform correlation matrix and antenna positions for MIMO radar transmit beampattern formation," *IEEE Sensors Journal*, vol. 20, no. 13, pp. 7326–7336, 2020.

[11] R. Z. Syeda, T. G. Savelyev, M. C. van Beurden, and A. B. Smolders, "Sparse MIMO array for improved 3D mm- Wave imaging radar," in *2020 17th European Radar Conference (EuRAD)*, 2021, pp. 342–345.

[12] M. Alaee-Kerahrood, P. Babu, and M. Soltanalian, *Signal Design for Modern Radar Systems*. Artech House, 2022.

[13] E. Raei, M. Alaee-Kerahroodi, P. Babu, and M. R. B. Shankar, "Design of MIMO radar waveforms based on lp-Norm criteria," 2021.

[14] C. Vasanelli, R. Batra, A. D. Serio, F. Boegelsack, and C. Waldschmidt, "Assessment of a Millimeter-Wave antenna system for MIMO radar applications," *IEEE Antennas and Wireless Propagation Letters*, vol. 16, pp. 1261–1264, 2017.

[15] P. M. McCormick, S. D. Blunt, and J. G. Metcalf, "Wideband MIMO Frequency-Modulated emission design with space-frequency nulling," *IEEE Journal of Selected Topics in Signal Processing*, vol. 11, no. 2, pp. 363–378, 2017.

[16] R. Amar, M. Alaee-Kerahroodi, and M. R. Bhavani Shankar, "FMCW-FMCW interference analysis in mm-wave radars; an indoor case study and validation by measurements," in *2021 21st International Radar Symposium (IRS)*, 2021, pp. 1–11.

[17] H. Sun, F. Brigui, and M. Lesturgie, "Analysis and comparison of MIMO radar waveforms," in *2014 International Radar Conf.*, 2014, pp. 1–6.

[18] Y. Sun, M. Bauduin, and A. Bourdoux, "Enhancing Unambiguous velocity in Doppler-Division Multiplexing MIMO radar," in *2021 18th European Radar Conference (EuRAD)*, 2022, pp. 493–496.

[19] A. Zwanetski and H. Rohling, "Continuous wave MIMO radar based on time division multiplexing," in *2012 13th International Radar Symposium*, 2012, pp. 119–121.

[20] J. Jung, S. Lim, S.-C. Kim, and S. Lee, "Solving Doppler-Angle Ambiguity of BPSK-MIMO FMCW Radar system," *IEEE Access*, vol. 9, pp. 120 347–120 357, 2021.

[21] A. B. Baral and M. Torlak, "Joint Doppler Frequency and Direction of Arrival Estimation for TDM MIMO Automotive Radars," *IEEE Journal of Selected Topics in Signal Processing*, vol. 15, pp. 980–995, 2021.

[22] F. Xu, S. A. Vorobyov, and F. Yang, "Transmit Beamspace DDMA Based Automotive MIMO Radar," *IEEE Trans. Veh. Teclnol.*, vol. 71, no. 2, pp. 1669–1684, 2022.

[23] R. Feger, C. Pfeffer, and A. Stelzer, "A Frequency-Division MIMO FMCW Radar System Based on Delta–Sigma Modulated Transmitters," *IEEE Transactions on Microwave Theory and Techniques*, vol. 62, no. 12, pp. 3572–3581, 2014.

[24] F. Yang, F. Xu, X. Yang, and Q. Liu, "DDMA MIMO radar system for low, slow, and small target detection," *The Journal of Engineering*, vol. 2019, no. 19, pp. 5932–5935, 2019.

[25] F. Jansen, "Automotive Radar Doppler Division MIMO With Velocity Ambiguity Resolving Capabilities," in *2019 16th European Radar Conference (EuRAD)*, 2019, pp. 245–248.

[26] M. Q. Nguyen, R. Feger, J. Bechter, M. Pichler-Scheder, M. H. Hahn, and A. Stelzer, "Fast-Chirp FDMA MIMO Radar System Using Range-Division Multiple-Access and Doppler-Division Multiple-Access," *IEEE Transactions on Microwave Theory and Techniques*, vol. 69, no. 1, pp. 1136–1148, 2021.

[27] O. Bialer, A. Jonas, and T. Tirer, "Code optimization for fast chirp FMCW automotive MIMO radar," *IEEE Trans. Veh. Teclnol.*, vol. 70, no. 8, pp. 7582–7593, 2021.

[28] W. van Rossum and L. Anitori, "Doppler ambiguity resolution using random slow-time code division multiple access MIMO radar with sparse signal processing," in *2018 IEEE Radar Conference (RadarConf18)*, 2018, pp. 0441–0446.

[29] M. Alaee-Kerahroodi, A. Aubry, A. De Maio, M. M. Naghsh, and M. Modarres-Hashemi, "A coordinate-descent framework to design low PSL/ISL sequences," *IEEE Trans. Signal Process.*, vol. 65, no. 22, pp. 5942–5956, Nov. 2017.

[30] M. Alaee-Kerahroodi, M. Modarres-Hashemi, and M. M. Naghsh, "Designing sets of binary sequences for MIMO radar systems," *IEEE Trans. Signal Process.*, vol. 67, no. 13, pp. 3347–3360, July 2019.

[31] L. Wu, M. Alaee-Kerahroodi, and B. M. R. Shankar, "Improving pulse-compression weather radar via the joint design of subpulses and extended mismatch filter," in *IGARSS 2022 - 2022 IEEE International Geoscience and Remote Sensing Symposium*, 2022, pp. 469–472.

[32] R. Amar, M. Alaee-Kerahroodi, P. Babu, and B. S. M. R., "Designing interference-immune doppler-tolerant waveforms for radar systems," *IEEE Trans. on Aerospace and Electronic Systems*, pp. 1–20, 2022.

[33] E. Raei, M. Alaee-Kerahroodi, and M. B. Shankar, "Spatial- and Range- ISLR trade-off in MIMO Radar Via Waveform C—orrelation optimization," *IEEE Transactions on Signal Processing*, vol. 69, pp. 3283–3298, 2021.

[34] E. Raei, S. Sedighi, M. Alaee-Kerahroodi, and M. B. Shankar, "MIMO radar transmit beampattern shaping for spectrally dense environments," *IEEE Trans. Aerosp. Electron. Syst*, pp. 1–13, 2022.

[35] A. E. Ertan, K. Anderson, and M. Ali, "Cognitive radar approaches to address interference mitigation in mobility applications," in *2022 IEEE Radar Conference (RadarConf22)*, 2022, pp. 1–6.

[36] J. Overdevest, F. Jansen, F. Uysal, and A. Yarovoy, "Doppler influence on waveform orthogonality in 79 GHz MIMO phase-coded automotive radar," *IEEE Trans. Veh. Teclnol.*, vol. 69, no. 1, pp. 16–25, 2020.

[37] W. Rowe, P. Stoica, and J. Li, "Spectrally constrained waveform design [SP tips tricks]," *IEEE Signal Processing Magazine*, vol. 31, no. 3, pp. 157–162, 2014.

[38] P. Stinco, M. Greco, F. Gini, and B. Himed, "Cognitive radars in spectrally dense environments," *IEEE Aerospace and Electronic Systems Magazine*, vol. 31, no. 10, pp. 20–27, 2016.

[39] M. Labib, V. Marojevic, A. F. Martone, J. H. Reed, and A. I. Zaghloui, "Coexistence between communications and radar systems: A survey," *URSI Radio Science Bulletin*, vol. 2017, no. 362, pp. 74–82, 2017.

[40] M. Alaee-Kerahroodi, K. V. Mishra, M. R. Bhavani Shankar, and B. Ottersten, "Discrete-phase sequence design for coexistence of MIMO radar and MIMO communications," in *2019 IEEE 20th International Workshop on Signal Processing Advances in Wireless Communications (SPAWC)*, 2019, pp. 1–5.

[41] L. Zheng, M. Lops, Y. C. Eldar, and X. Wang, "Radar and communication coexistence: An overview: A review of recent methods," *IEEE Signal Processing Magazine*, vol. 36, no. 5, pp. 85–99, 2019.

[42] B. Tang and J. Li, "Spectrally constrained MIMO radar waveform design based on mutual information," *IEEE Trans. Signal Process.*, vol. 67, no. 3, pp. 821–834, 2019.

[43] C. Vasanelli, R. Batra, and C. Waldschmidt, "Optimization of a MIMO radar antenna system for automotive applications," in *2017 11th European Conference on Antennas and Propagation (EUCAP)*, 2017, pp. 1113–1117.

[44] D. W. Bliss, K. W. Forsythe, and C. D. Richmond, "MIMO radar: Joint array and waveform optimization," in *2007 Conference Record of the Forty-First Asilomar Conference on Signals, Systems and Computers*, 2007, pp. 207–211.

[45] Z. Cheng, Y. Lu, Z. He, Yufengli, J. Li, and X. Luo, "Joint optimization of covariance matrix and antenna position for MIMO radar transmit beampattern matching design," in *2018 IEEE Radar Conference (RadarConf18)*, 2018, pp. 1073–1077.

[46] M. Soltanalian, B. Tang, J. Li, and P. Stoica, "Joint design of the receive filter and transmit sequence for active sensing," *Signal Processing Letters, IEEE*, vol. 20, no. 5, pp. 423–426, 2013.

[47] E. K. Ghafi, S. A. Ghorashi, and E. Mehrshahi, "Reconfigurable linear antenna arrays for beam-pattern matching in collocated MIMO radars," *IEEE Trans. Aerosp. Electron. Syst*, vol. 57, no. 5, pp. 2715–2724, 2021.

[48] H. He, J. Li, and P. Stoica, *Waveform design for active sensing systems: a computational approach*. Cambridge University Press, 2012.

[49] H. He, P. Stoica, and J. Li, "Designing unimodular sequence sets with good correlations; including an application to MIMO radar," *IEEE Trans. Signal Process.*, vol. 57, no. 11, pp. 4391–4405, Nov. 2009.

[50] G. Cui, X. Yu, M. Piezzo, and L. Kong, "Constant modulus sequence set design with good correlation properties," *Signal Processing*, vol. 139, pp. 75–85, 2017.

[51] Y. Li and S. A. Vorobyov, "Fast algorithms for designing unimodular waveform(s) with good correlation properties," *IEEE Trans. Signal Process.*, vol. 66, no. 5, pp. 1197–1212, Mar. 2018.

[52] J. Song, P. Babu, and D. P. Palomar, "Sequence set design with good correlation properties via majorization-minimization," *IEEE Trans. Signal Process.*, vol. 64, no. 11, pp. 2866–2879, June 2016.

[53] M. Alaee-Kerahroodi, M. R. Bhavani Shankar, K. V. Mishra, and B. Ottersten, "Meeting the lower bound on designing set of unimodular sequences with small aperiodic/periodic ISL," in *2019 20th International Radar Symposium (IRS)*, 2019, pp. 1–13.

[54] E. Raei, M. Alaee-Kerahroodi, and M. Bhavani Shankar, "Waveform design for Range-ISL minimization with spectral compatibility in MIMO radars," in *2022 19th European Radar Conf.*, 2022, pp. 101–104.

[55] S. Shi, Z. Wang, Z. He, and Z. Cheng, "Spectrally compatible waveform design for MIMO radar with ISL and PAPR constraints," *IEEE Sensors Journal*, vol. 20, no. 5, pp. 2368–2377, 2020.

[56] Z. Cheng, Z. He, M. Fang, J. Li, and J. Xie, "Spectrally compatible waveform design for MIMO radar transmit beampattern with PAR and similarity constraints," in *2018 IEEE International Conf. on Acoustics, Speech and Signal Processing (ICASSP)*, 2018, pp. 3286–3290.

[57] M. Alaee-Kerahroodi, E. Raei, S. Kumar, and M. Bhavani Shankar, "Cognitive radar waveform design and prototype for coexistence with communications," *IEEE Sensors Journal*, pp. 1–1, 2022.

[58] M. Deng, Z. Cheng, and Z. He, "Spectrally Compatible Waveform Design for Large-Scale MIMO Radar beampattern synthesis with One-Bit DACs," *IEEE Transactions on Aerospace and Electronic Systems*, vol. 58, no. 5, pp. 4729–4744, 2022.

[59] M. Alaee-Kerahroodi, L. Wu, E. Raei, and M. R. B. Shankar, "Joint waveform and receive filter design for pulse compression in weather radar systems," *IEEE Transactions on Radar Systems*, vol. 1, pp. 212–229, 2023.

[60] X. Yu, H. Qiu, J. Yang, W. Wei, G. Cui, and L. Kong, "Multi-spectrally constrained MIMO radar beampattern design via sequential convex approximation," *IEEE Transactions on Aerospace and Electronic Systems*, vol. 58, pp. 1–1, 08 2022.

[61] N. K. Sichani, M. Alaee-Kerahroodi, B. Shankar, E. Mehrshahi, and S. A. Ghorashi, "Waveform design for 4D-imaging mmWave PMCW MIMO radars with spectrum compatibility," in *2023 20th European Radar Conference (EuRAD)*, 2023, pp. 110–113.

[62] J. Li and P. Stoica, *Adaptive Signal Design For MIMO Radars*. Wiley, 2009, pp. 193–234.

[63] "Design guide: TIDEP -01012—Imaging radar using cascaded mmWave sensor reference design (REV. A)," Texas Instruments Inc., Dallas , 2019, [Online]. Available: http://www.ti.com/lit/ug/tiduen5a/tiduen5a.pdf.

[64] "Vayyar 4D Imaging Radar on Chip," [Online]. Available:, https://vayyar.com/technology/#hardware.

[65] A. Ganis, E. M. Navarro, B. Schoenlinner, U. Prechtel, A. Meusling, C. Heller, T. Spreng, J. Mietzner, C. Krimmer, B. Haeberle, S. Lutz, M. Loghi, A. Belenguer, H. Esteban, and V. Ziegler, "A portable 3-D imaging FMCW MIMO radar demonstrator with a 24×24 antenna array for medium-range applications," *IEEE Transactions on Geoscience and Remote Sensing*, vol. 56, no. 1, pp. 298–312, 2018.

[66] K. E. Dungan, C. D. Austin, J. W. Nehrbass, and L. C. Potter, "Civilian vehicle radar data domes," in *Defense + Commercial Sensing*, 2010.

Nazila Karimian-Sichani received the B.Sc. and M.Sc. degrees in electrical engineering from the Isfahan University of Technology, Esfahan, Iran, in 2012 and 2014, respectively. She started the Ph.D. degree in electrical communication systems at Shahid Beheshti University, Tehran, Iran, in 2018. She has joined the Signal Processing Application in Radar and Communications (SPARC) group, Interdisciplinary Centre for Security, Reliability, and Trust (SnT), University of Luxembourg, as a Visiting Researcher, from 2022 to 2023. Since 2023, she has joined the university of Pisa as a research associate. Her research interests include waveform optimization and array design for automotive radar applications.

Mohammad Alaee-Kerahroodi is an IEEE senior member who received his PhD in telecommunication engineering from Isfahan University of Technology's Department of Electrical and Computer Engineering in 2017. In 2016, he was a visiting researcher at the University of Naples "Federico II" in Italy. Following his degree, he worked as a research associate at the Interdisciplinary Centre for Security, Reliability, and Trust (SnT) at the University of Luxembourg in Luxembourg. He is currently a research scientist at SnT, where he coordinates the SPARC (Signal Processing Applications in Radar and Communications) research group's prototype and laboratory activities. His research focuses on radar waveform design and array signal processing, with a particular emphasis in creating novel solutions for millimeter wave MIMO radar sensors capable of 4D imaging. Dr. Alaee brings an array of practical expertise to his research, having worked actively with various radar systems for over 12 years. His knowledge includes automotive radar, ground surveillance radar, air surveillance radar, weather monitoring radar, passive sensing radar, and marine radar applications.

M. R. Bhavani Shankar received Masters and Ph. D in Electrical Communication Engineering from Indian Institute of Science, Bangalore in 2000 and 2007 respectively. He was a Post Doc at the ACCESS Linnaeus Centre, Signal Processing Lab, Royal Institute of Technology (KTH), Sweden from 2007 to September 2009. He joined SnT in October 2009 as a Research Associate and is currently a Senior Research Scientist/ Assistant Professor at SnT leading the SPARC (Signal Processing Applications in Radar and Communications). He was with Beceem Communications, Bangalore from 2006 to 2007 as a Staff Design Engineer working on Physical Layer algorithms for WiMAX compliant chipsets. He was a visiting student at the Communication Theory Group, ETH Zurich, headed by Prof. Helmut Bölcskei during 2004. Prior to joining Ph. D, he worked on Audio Coding algorithms in Sasken Communications, Bangalore as a Design Engineer from 2000 to 2001. His research interests include Design and Optimization of MIMO Communication Systems, Automotive Radar and Array Processing, polynomial signal processing, Satellite communication systems, Resource Allocation and Fast Algorithms for Structured Matrices. He is currently the Chair of the IEEE Benelux joint chapter on communications and vehicular technology, member of the Sensor Array Mulichannel (SAM) Technical Committee of Signal Processing Society, serves as handling editor for Elsevier Signal Processing and member of the EURASIP Technical Area Committee on Theoretical and Methodological Trends in Signal Processing. He was a co-recipient of the 2014 Distinguished Contributions to Satellite Communications Award, from the Satellite and Space Communications Technical Committee of the IEEE Communications Society.

Esfandiar Mehrshahi received his B.Sc. degree from the Iran University of Sicience and Technology, Tehran, Iran, in 1987, and the M.Sc. and Ph.D. degrees from the Sharif University of Technology, Tehran, Iran, in 1991 and 1998, respectively, all in Electrical Engineering. Since 1990, he has been involved in several research and engineering projects at the Iran Telecommunications Research Center (ITRC). He is currently an associated professor at Shahid Beheshti University (SBU), Tehran, Iran. His main areas of interest are the nonlinear simulation of microwave circuits, low phase noise oscillators, and computational electromagnetics.

Seyed Ali Ghorashi , senior member of IEEE, earned both the B.Sc. and M.Sc. degrees in Electrical Engineering from the University of Tehran, followed by a Ph.D. from King's College London, U.K. He has worked at Samsung Electronics Ltd. (U.K.), Shahid Beheshti University, Middlesex University, and the University of East London. Possessing international patents with a publication record exceeding 120 technical papers, his research primarily revolves around the applications of optimization, artificial intelligence, and machine learning in positioning, the Internet of Things (IoT), Human Activity Recognition (HAR) and wireless communications.